On the Hopf bifurcation and Landau-Stuart constants associated with vortex 'shedding' behind circular cylinders

K.R. Sreenivasan, P.J. Strykowski* & D.J. Olinger
Mason Laboratory, Yale University, New Haven, CT 06520

We show by means of transient experiments that the bifurcation accompanying vortex 'shedding' behind circular cylinders is of the Hopf type, and that the Landau-Stuart equation describes the immediate post-critical behaviour quite well. We determine the Landau-Stuart constants, several of which are shown to be independent of the measurement position in the wake as well as the flow Reynolds number. We examine the sense in which absolute instability is relevant to the vortex 'shedding' problem, and argue that the wake dynamics in the neighbourhood of the critical Reynolds number is best described in terms of the spatial instability in the subcritical regime and of a global temporal instability in the supercritical regime.

Extended version of: "Hopf bifurcation, Landau constants and vortex shedding behind circular cylinders", by the same authors, ASME Forum on Unsteady Flow Separation, ed. K.N. Ghia, pp. 1-13, 198

* Present address: Department of Mechanical Engineering, University of Minnesota, Minneapolis, MN 55455.

1. Introduction

One of the thrusts of research in the last few years has been the search for 'universal' routes accompanying the evolution of a system to a complex state, and the exploration of whether the ensuing complexity can be modelled by low-dimensional equations or maps. In the context of fluid flows, this approach has had remarkable success in highly confined flows, the best example being the Rayleigh-Bénard convection in small aspect ratio cells. Two selected but representative references are Libchaber & Maurer (1981) and Jensen et al. (1985). It is not *à priori* clear whether this feature extends to the more general class of unconfined flows. This question has been addressed by us in the context of wakes, and some results have been reported in Sreenivasan (1985), Olinger & Sreenivasan (1988a,b), and Chhabra, Olinger & Sreenivasan (1989). This work takes a step back from our earlier work, and concentrates on the phenomenon of vortex 'shedding'* in the neighbourhood of the 'critical' Reynolds number.

It is well known that the flow behind circular cylinders is steady up to a certain critical Reynolds number. Beyond the critical value, the flow develops into a periodic state, corresponding to the formation behind the cylinder of two rows of staggered vortices of opposite sign – the so-called Kármán vortex 'street'**. Two specific points addressed here are the following. First, we establish by experiment the precise nature of the bifurcation occurring at the critical Reynolds number; we shall show that the bifurcation is strictly of the Hopf type. Landau (see, for example, Landau & Lifshitz 1959, p103, Stuart 1958, 1960) proposed a simple model equation to describe the post-critical state of a system undergoing supercritical bifurcation of the Hopf type. Our second purpose here is to make measurements specifically designed to answer the question of how well the Landau-Stuart equation describes the wake dynamics in the immediate post-critical state, and to determine the relevant Landau-Stuart constants.

---

* No specific physical process is implied by the use of the word 'shedding' which, for convenience, will be used subsequently without quotes.

**The downstream distance up to which this 'street' survives behind the cylinder depends on the Reynolds number (Cimbala, Nagib & Roshko 1988).

On the basis of the results to be described here and in the companion paper (Strykowski & Sreenivasan 1988 – to be referred to as II below), as well as the previous work mentioned above, it appears that the wake dynamics at low Reynolds numbers can be described rather precisely by low- dimensional temporal models. Particular reference must be made to the fact that the dynamics of the wake behind an oscillating cylinder at the so-called 'critical golden mean point' can be described to a large measure by the one-dimensional sine circle map (Olinger & Sreenivasan 1988a,b, Chhabra et al. 1989). It is not entirely clear why this should be so, given that there exists no deductive proof that such extremely simple maps are rational approximations to the Navier-Stokes equations. The work to be described here, namely that the *local* dynamics of the flow above the critical Reynolds number can be described by essentially temporal equations (§§4-6), gives some qualitative explanation for the success of such efforts. It has also been suggested (Huerre 1985, Sreenivasan & Ramshankar 1986) that an *a priori* condition for expecting some such scenario to hold is that the nature of the flow instability must be of the absolute type. The third objective of this work is to determine the sense in which the present measurements support the notion that the vortex shedding process in wakes is governed by absolute instability.

While the supercritical dynamics is governed by temporal characteristics, it appears that the subcritical dynamics is of the spatial type. A fourth purpose of this paper is to consolidate these views in some unified way. For this, the material in II forms a useful complement.

In §2, we briefly describe Hopf bifurcation and discuss the nature of measurements required to quantify it; although no direct inferences on Hopf bifurcation will be made until §5.6, its introduction in the beginning motivates the measurements reported in §4. The experimental set-up and instrumentation are described in §3. Section 5 describes the determination of the Landau constants. It has been known for a while that vortex shedding is accompanied by large amplitude pure-frequency oscillation; this was demonstrated perhaps most directly by Sreenivasan (1985) one of whose figures, reproduced here as figure 1, shows the sharpness of the spikes as well as their relative strength compared to the background. It has been suggested (Koch 1985, Huerre & Monkewitz 1985, Monkewitz & Nguyen 1986, Strkowski

1986, Hannemann & Oertel 1988, Sreenivasan, Raghu & Kyle 1989) that such pure frequency oscillations are charactersitic of absolute instability. We address in §6 the question of the relevance of absolute instability to the wake problem in the supercritical regime, and close with §7 summarizing the chief conclusions.

This work has earlier been presented by one of us (KRS) at an invited talk in the 1986 international meeting on Phase Space Dynamics organised at the University of Maryand, and written up in a preliminary version in Sreenivasan, Strykowski & Olinger (1987). Since completing part of this work in spring of 1985, and most of it by spring of 1986, we have come across two other papers (Mathis, Provansal & Boyer 1984, and Provansal, Mathis & Boyer 1987) whose contents overlap significantly with those reported here. However, on matters of instrumentation, emphasis and lines of inquiry, this work is different and detailed enough that an independent publication appeared appropriate; it also seemed desirable to provide a reinforcement where there was an overlap with previous work, and point out differences where they surfaced. A detailed comparison with this previous work is given in §5.7. The thesis of Strykowski (1986) to which Provansal et al. (1987) make reference is in fact summarized in this paper and in II.

2. Hopf bifurcation

We consider a disturbance superimposed on the steady basic state of a system. We first ignore all aspects of spatial dependence and consider only the temporal development of the disturbance; we shall review in §§5 and 6 the sense in which this is appropriate to the wake. We consider the case where the disturbance grows to reach a saturation amplitude when the basic system becomes unstable. The phase representation of this latter state is a limit cycle.

Let u_r and u_i be the real and imaginary parts of the perturbation velocity imposed on the steady state wake. If we plot the evolution of u_i and u_r against the Reynolds number Re, all perturbations below the critical Reynolds number Re_{cr} wind down to zero. If the bifurcation is of the Hopf type, small perturbations grow exponentially with time above Re_{cr}, and eventually asymptote to a finite amplitude $u_{os} \sim (Re - Re_{cr})^{1/2}$. Here, u_{os} is the saturation value of the

disturbance amplitude $u_o = (u_r^2 + u_i^2)^{1/2}$. The situation is illustrated in figure 2a. Further, writing in the linear stage

$$[u'] = [A]\,[u], \qquad (2.1)$$

with the dash denoting the time derivative, we require for Hopf bifurcation that the eigenvalues of the matrix A(Re) be complex conjugates, $\lambda_r \pm (\sqrt{-1})\lambda_i$, say, and reside in the left half of the complex plane for $Re < Re_{cr}$, and cross the imaginary axis at Re_{cr}, the speed at which the eigenvalues cross the imaginary axis, $d\lambda_r/dRe$, must be positive and finite (figure 2b). More details can be found, e.g., in Guckenheimer & Holmes (1983, p150).

Our objective is to quantify by measurement the growth of perturbations which eventually lead to vortex shedding. This can be done in principle by imposing a small disturbance on the steady state of the wake at different Reynolds numbers in the vicinity of the critical value, and determining the matrix A from the exponential stage of the disturbance growth. But in experiments at Reynolds numbers above the critical value, such steady states are inaccessible except through transient experiments in which the flow at any desired Reynolds number is created suddenly from rest. The flow then evolves through a 'quasi-steady' state (as in the numerical simulations of Hannemann 1987 and Hannemann & Oertel 1988) which can then be considered to have been perturbed by the background disturbances present in the flow facility. The perturbation does not grow if the flow is subcritical, and the only observable asymptotic state is the steady one. If, on the other hand, the flow is supercritical, the background fluctuations grow, and a new state ensues. The linear as well as the nonlinear stages of evolution to this new state concerns us here.

3. Experimental facilities and instrumentation

3.1 Wind Tunnels

Measurements were made in pressure driven wind tunnels, supplied with compressed dry air from two large storage tanks (combined storage volume of approximately 18 m^3 at a storage pressure of 8×10^5 N/m^2). One of the tunnels was a carefully designed, low turbulence

3.2 The cylinders

Well polished drill rods were fitted with end plates to allow variation in aspect ratio and to provide better end conditions; the plates were designed following Stansby (1974). Detailed measurements were made at aspect ratios, L/D, of 60, 27 and 14. A summary of the relevant diameters, aspect and blockage ratios is given in table 1.

3.3 Instrumentation

Some of the results to follow were obtained with DANTEC constant temperature hot-wire anemometers, type 55M01, using 5μm wires etched to a working length of approximately 0.8mm; overheat ratios of 1.75 were used. The resulting data were DC offset and filtered with a DANTEC signal conditioner, model 55D26, and amplified to optimize the 12-bit resolution (±5 Volts) of the MASSCOMP MC-5000 series computer. All data processing was done on this machine. During the initial stages of the work, it was felt that the hot-wire probe, when placed within a few diameters of the cylinder, might be intruding with some details of flow development (see Kovasznay 1949, Mair & Maull 1971, and II). Thus, all hot-wire measurements were made outside of this sensitive region. Within this region, velocity measurements were made with a TSI laser Doppler velocimeter (LDV) in the forward scatter mode. In instances where both LDV and hot-wire were deemed reliable, both were used under identical circumstances as a check on each other.

Mean velocity was obtained using a Pitot-tube and an MKS-Baratron unit with a 10 Torr differential pressure head.

4. Principal experimental results

4.1 Temporal growth rates

Let us first concentrate on the growth rates of the disturbances at some supercritical Reynolds number. The experiments needed to determine these growth rates must consist of abruptly setting the flow at the desired Reynolds number, and observing how the oscillations

grow in time. If the disturbance (at any given position) amplifies exponentially as one expects to be the case initially, one can obtain the growth rate a_r from

$$u_o \sim \exp(a_r t). \tag{4.1}$$

If the growth rates are the same everywhere in a finite region of the flow, the perturbation grows temporally everywhere in that region.

The globe valve mentioned in §3.1.2 was opened suddenly, and the streamwise velocity signal at the chosen location within the wake was digitally recorded either by the hot-wire or LDV. Linearization of hot-wire signals was done in some cases, but since this did not produce significant differences, many experiments were made without linearizing. To obviate unnecessary changes in the mass flow rate, and to improve the effective time constant for the rise time of the mean velocity, the flow rate was increased from a value slightly below Re_{cr} (where only background fluctuations were present) to the desired supercritical Reynolds number at which the oscillations selected by the flow begin to grow from the background.

A typical mean velocity change as well as an oscillogram of velocity fluctuations are given in figure 3. The accompanying flow Reynolds number variation in the top trace is from 43 to 49, occurring in a time scale of the order of 200 msec. The bottom trace (b) shows the manner in which the oscillations in the streamwise velocity, measured at x/D = 10, y/D = 1, grow with time. The signal in figure 3(a) was low pass filtered below 30 Hz so as to reflect only the mean velocity variations, while the trace in figure 3(b) was high pass filtered above 30 Hz to remove the mean velocity variation. The vortex shedding frequency was about 48 Hz, so that this high pass filtering did not introduce too much phase or frequency modifications in the oscillations. The mean and fluctuation responses in figure 3 were recorded simultaneously, but by two different hot-wires arranged in a non-intrusive way: The one used to obtain the mean flow response was placed slightly upstream of the cylinder, and so a time shift due to convection, of approximately 40 msec., must be made before comparing figures 3(a) and 3(b). The oscillations commence only after the Reynolds number attains the supercritical value; hence, it is clear that the characteristics of the oscillations correspond unambiguously to this

supercritical state. This behaviour was observed even at those supercritical Reynolds numbers for which the characteristic growth time of the oscillations was comparable or smaller than the rise time of the mean velocity. Presumably, oscillations do not amplify at the intermediate supercritical states because the instability associated with such tarnsient states does not have time to develop.

The amplitude of the envelope in figure 3(b) can now be processed to obtain the growth rates. The logarithm of the amplitude envelope (figure 4a) plotted against time in figure 4(b) shows a linear region whose slope gives the constant a_r in (4.1) at the Reynolds number corresponding to the upper plateau in figure 3a.

LDV measurements made at 5 diameters downstream of the cylinder show exactly the same features. It should be noted that as one gets closer to the cylinder than, say, 2.5 diameters, the growth rate measurements become more and more uncertain; some of the anomalies observed are not understood, and will not be discussed here.

All the growth rate measurements were made in the shear layer region of the wake (that is, the region in which only one frequency is apparent in the hot-wire or LDV signals). If one moves closer to the cylinder axis, the influence of the opposite row of vortices will be felt, and the observed frequency will acquire a dominant harmonic component. In such cases, the exponential growth rates can be fitted for each of the frequencies separately. We have done this, and especially examined the growth rates on the centerline. However, further consideration of this feature is best relegated until after the basic facts have been established (see §5.4).

4.2 Decay rates

While the measurement of growth rates is a relatively straightforward, the same cannot be said of decay rates. In determining growth rates, we set the flow instantly (in principle) to the required supercritical Reynolds number starting from some subcritical state. Since the latter does not possess any preferentially periodic oscillations, the flow is free to choose the frequency and amplitudes appropriate to the supercritical Reynolds number. In contrast, decay

measurements require the examination of the wake response in the subcritical state, where periodic oscillations can be established only by means of some external forcing. The correct procedure would therefore be to establish (by some external means) flow oscillations at the *right* frequency appropriate to the desired subcritical Reynolds number, and switch off the forcing to quantify the ensuing decay of the oscillations. One does not *a priori* know what this right forcing frequency should be (or, for that matter, whether such a frequency exists), and how the decay rates depend on this frequency; part of the work reported in this subsection concerns these questions.

Flow oscillations in the subcritical states were set up in three different ways. In the first two, oscillations were set up at the desired subcritical Reynolds number by either: (a) mechanically oscillating the cylinder, or (b) acoustically exciting flow oscillations behind the stationary cylinder. The source of excitation was then switched off abruptly, and the decay of flow oscillations in the wake was recorded. In the third method (c), a steady flow was set up at a slightly supercritical Reynolds number Re^+ so that full-fledged oscillations occurred naturally. The flow was suddenly slowed down to the desired subcritical Reynolds number Re^- below Re_{cr}, and the ensuing decay rates of the oscillations was measured. These decay rates were then taken to correspond to the Reynolds number Re^-. Clearly, this is a reasonable procedure if Re^+ is close to Re^- (or, we are in the very close vicinity of Re_{cr}). For $(Re^+ - Re^-)$ not small, in so far as the initial oscillations are at a frequency characteristic of Re^+ and not of Re^-, the results can only be considered approximate. However, there is an important reason for these measurements to which we shall return in §5.3; we shall also have occasion to refer to these measurements in §5.2. The primary point to be made here is that the decay rates of wake oscillations were observed to be exponential in all these cases (see figure 5 for an example), and the coefficient a_r in equation (4.1) was obtained as for the growth case – the difference, of course, being that a_r is negative during decay.

We tried several excitation frequencies in methods (a) and (b). Our first choice was the frequency which showed the largest *spatial* growth in the steady basic state below Re_{cr}; from the work of Nishioka & Sato (1978), we know that forcing at this special frequency (fD/U_o =

0.1) can indeed set up vortex shedding below Re_{cr}. (See also Taneda 1963, and Berger 1964.) Oscillations could be set up at other frequencies also, but at these other frequencies the amount of external excitation required to produce sizeable flow oscillations is larger. We have used as an example the frequency corresponding to a backward extrapolation of Roshko's (1954) relation

$$f_s D^2/\nu = 0.212\,Re - 4.5, \tag{4.2}$$

f_s being the vortex shedding frequency. In this case too, the decay rates following the removal of the cylinder excitation were exponential as before.

Interestingly, we could not excite oscillations in the wake (say, in the region $x/D > 7$) when the Reynolds number was below *about* 25, even with strong external excitation. Nishioka & Sato (1978) remarked similarly, but thier work puts this number around a slightly different value of 20. We believe that this limiting Reynolds number, which must be calculable by energy methods of the sort discussed in Joseph (1976), forms another critical value below which perturbations, no matter how large, cannot be sustained in the wake. A related remark will be made in §6.2.

The measured growth and decay rates are collected in figure 6. Only one set of growth rate data has been plotted, but other sets obtained at different x/D (by LDV as well as hot-wires) were no different (see inset to figure 6), except that the measurement uncertainty was larger at downstream distances, both because of the smaller amplitudes and somewhat higher three-dimensional effects there. It is clear that the exponent a_r varies linearly with the Reynolds number in a certain nontrivial neighborhood of Re_{cr} which, by definition, is the Reynolds number at which $a_r = 0$.

The main conclusion from figure 6 is that

$$Re_{cr} \approx 46 \tag{4.3a}$$

and that there exists a certain non-trivial neighborhood of Re_{cr} in which the growth and decay

rates behave according to

$$d(a_r D^2/\nu)/dRe \approx 0.2. \qquad (4.3b)$$

(The reason for normalizing the growth and decay rate data in figure 6 by the viscous time scale D^2/ν instead of the convective time scale D/U_o is simply that $a_r D^2/\nu$ is usually of the order unity while $a_r D/U_o$, which is smaller by the factor of the Reynolds number, gives numerical values on the order 0.01.) As already mentioned, *the results (4.3a) and (4.3b) are independent of the measurement location.* Another important points is that the decay rates are independent of the excitation frequency. This may not be completely evident from the scatter in figure 6, but least square fits to several sets of decay data (obtained at the two excitation frequencies already mentioned, as well as by the two different methods of excitation) agreed with (4.3b) to within about 8%.

The growth and decay rates vary with the aspect ratio of the cylinder. Detailed growth rate measurements were made for aspect ratios of 60, 27 and 14 (figure 7), but the corresponding decay rate measurements were less detailed except for the aspect ratio of 60. Obviously, the critical Reynolds number corresponding to zero growth rate is seen to be a function of the aspect ratio, as has been pointed out, for example, by Nishioka & Sato (1974). For the aspect ratios mentioned above, the critical Reynolds numbers were respectively 46, 50 and 53, in reasonable agreement with the data of Nishioka & Sato. We satisfied ourselves that the critical Reynolds number for the aspect ratio of 200 was also 46 in the present facilities, and therefore concluded that the results for the aspect ratio of 60 represent the essentials of the phenomena for an infinitely long cylinder. Time-dependent numerical simulations by Strykowski (briefly described in II, but yet unpublished in detail) of two-dimensional Navier-Stokes equations verify the temporal exponential growth* of fluctuations in the supercritical regime, and indicate preliminary values of $Re_{cr} = 41$ and

---

* Since the background noise in numerical calculations is much smaller than in experiments, the exponential growth can be observed over several decades of amplitude growth.

$d(a_r D^2/\nu)/dRe = 0.24$. Numerical stability calculations by Jackson (1987) of two-dimensional eigenfunctions predict a critical Reynolds number of 46.2 for the two-dimensional circular cylinder.

Oscillations grow rather slowly in very close positive vicinity of Re_{cr}; it is exciting to watch sustained oscillations appear just above Re_{cr}, say $Re_{cr} + 0.1$. The growth rates there are so small that saturation amplitudes are reached only for long times of the order of a minute corresponding to about 10^4 convective time scales D/U_0. Many flow facilities do not have test sections that are 10^4 cylinder diameters long, and it is therefore clear that the appearance of sustained pure-frequency oscillations at these Reynolds numbers cannot be related to any spatial development in the flow. In a few cases, we observed the growth phase extending forover one minute followed by an immediate decay over a comparable period of time, apparently because the Reynolds number had inadvertently fallen from just above to just below Re_{cr}.

4.3 The saturation amplitude

After the initial growth period, the amplitude saturates to a final value (see for example figure 3b). This final amplitude can be measured as a function of the flow Reynolds number. For data obtained at a fixed location in the wake, figure 8 shows that the square of this amplitude is a linear function of Re. Again, the intercept on the Reynolds number axis gives us another estimate of the critical Reynolds number; not surprisingly, this estimate agrees well with (4.3a). Since the saturation amplitude at fixed Reynolds number is different at different spatial positions (see, for example, Kovasznay 1949), the precise slope of the straight line in figure 8 varies with the spatial position in the wake. However, the linear relationship between the saturation amplitude and the Reynolds number was found to be true (to within measurement accuracy) at all positions in the wake where measurements were made.

5 The periodic (vortex shedding) state and the Landau equation

5.1 Two elementary features

It will now be shown that the results of the previous section are consistent with the dictates of the Landau, or Landau-Stuart, equation, whose further consequences we deduce and examine for consistency with measurements. The equation is meant to model some universal features of an unstable system in some finite (but small) vicinity of the critical Reynolds number, and has the form

$$\mathrm{d}\mathbf{u}/\mathrm{d}t = \mathbf{a}\,\mathbf{u} - \mathbf{c}\,|\mathbf{u}^2|\,\mathbf{u} \qquad (5.1)$$

where $\mathbf{u}$ is the (complex) velocity fluctuation, and $\mathbf{a}$ and $\mathbf{c}$ are both (in general) complex constants. Writing $\mathbf{u} = u_o \exp[i\phi(t)]$ we have:

$$\mathrm{d}u_o/\mathrm{d}t = a_r u_o - c_r u_o^3 \qquad (5.2)$$

governing the real part, and

$$\mathrm{d}\phi/\mathrm{d}t = a_i - c_i\, u_o^2 \qquad (5.3)$$

governing the imaginary part; the subscripts r and i indicate real and imaginary parts respectively. Equation (5.1) can be solved exactly (see Landau & Lifshitz 1959, p. 103), but our purposes are served adequately by noting the following features. Focusing first on (5.2), it is clear that all stable states correspond to $a_r < 0$ and $c_r > 0$. The second term on the right side is negligible in the linear regime and, as the basic state becomes unstable at Re_{cr}, the constant a_r will change sign from negative to positive: The disturbance will grow in the usual exponential manner at the rate a_r. As the amplitude increases, nonlinear effects lead to an amplitude saturation given by the condition $\mathrm{d}u_o/\mathrm{d}t = 0$ in (5.2), or

$$u_{os} = (a_r / c_r)^{1/2}. \qquad (5.4)$$

Following Landau, we may use Taylor's series and write a_r in the neighbourhood of Re_{cr} as:

$$a_r(Re) = a_r(Re_{cr}) + da_r/dRe\ (Re - Re_{cr}) + \ldots \qquad (5.5)$$

Since $a_r(Re_{cr}) = 0$ by definition, we have

$$a_r(Re) = da_r/dRe\ (Re - Re_{cr}). \qquad (5.6)$$

That is, the growth (or decay) rates are a linear function of the Reynolds number in the vicinity of Re_{cr} – as observed in the experiments (see figure 6 and equation (4.3b)). The fact that da_r/dRe is an absolute constant (equal to $0.2\nu/D^2$), *independent of the spatial position and Reynolds number,* is one of the important findings of this paper. Combining (5.6) with (5.4), we obtain the expression

$$u_{os}^2 = (1/c_r)\ da_r/dRe\ (Re - Re_{cr}). \qquad (5.7)$$

In general, c_r can also be expected to be a function of the Reynolds number, and a Taylor series expansion can be made in the vicinity of Re_{cr}. Equation (5.7) then yields

$$u_{os}^2 = (1/c_{ro})\ da_r/dRe\ (Re - Re_{cr}) - \frac{da_r/dRe\ (Re - Re_{cr})^2\ dc_r/dRe}{c_{ro}^2 + dc_r/dRe(Re - Re_{cr})c_{ro}} \qquad (5.8)$$

where $c_{ro} = c_r(Re_{cr})$. If

$$c_{ro} >> dc_r/dRe\ (Re - Re_{cr}), \qquad (5.9)$$

the first term on the right hand side of (5.8) is an adequate representation of u_{os}^2 in the supercritical regime, and we have

$$u_{os} = (1/c_{ro})^{1/2}\ (da_r/dRe)^{1/2}\ (Re - Re_{cr})^{1/2}. \qquad (5.10)$$

This states that the saturation amplitude increases as the half power of the difference Reynolds number $(Re - Re_{cr})$. Note that, unless dc_r/dRe is indeed small, the condition (5.9) will not be valid except in the immediate vicinity of Re_{cr}, but we saw in §4.3 that (5.10) is

valid over a finite range of $(Re - Re_{cr})$, implying that dc_r/dRe is indeed negligible. Expressions (5.6) and (5.7) suggest that the constants da_r/dRe and c_{ro} can be determined if the growth rates a_r and the saturation amplitudes u_{os} can be measured as a function of Re in the vicinity of Re_{cr}. This is precisely what we did in §4. Note that da_r/dRe is independent of the spatial position in the wake, but c_{ro} must be position- dependent because the saturation amplitude is so. One can obtain a qualitative appreciation for the magnitude variations of c_{ro} by perusing the saturation amplitude measurements of Kovasznay (1949) and Nishioka & Sato (1978). We shall remark on some representative values in §5.5.

5.2 The relation between the oscillation frequency and the Reynolds number

To determine the constants a_i and c_i, we turn to the imaginary part of (5.1). Noting that $d\phi/dt = 2\pi f$, where f is the oscillation frequency in the disturbed state, we may write (5.3) as

$$2\pi f = a_i - c_i u_o^2. \qquad (5.11)$$

If this is valid for the present problem, the following situation must occur; for convenience, we first concentrate on the supercritical regime postpone a discussion of the subcritical state until the next subsection. The oscillation frequency must equal $a_i/2\pi$ at the onset, and increase quadratically with the amplitude; the frequency shift depends on the second term involving c_i and denotes a nonlinear effect; if $c_i = 0$, the frequency selection in the supercritical wake is completely governed by the linear theory. The experimentally determined relation between the oscillation frequency and amplitude (figure 9) appears to validate this quadratic relation, and suggest that the linear theory becomes increasingly incapable predicting the frequency selection as the Reynolds number departs from the critical value. Below, we examine both the onset value of the oscillation frequency and its nonlinear variation.

The intercept in figure 9 gives the constant a_i appropriate to the measurement Reynolds number; this, of course, is the onset frequency f_o, and can be written as

$$f_o D^2/\nu = a_i D^2/(2\pi\nu) = a_{io} D^2/(2\pi\nu) + (1/2\pi)\,[d(a_i D^2/\nu)/dRe]\,(Re - Re_{cr}) \quad (5.12)$$

where $a_{io} = a_i(Re_{cr})$. The onset frequency obtained at various Reynolds numbers from figures such as 9 may now be plotted as in figure 10 to give a_{io} (the intercept) as well as da_i/dRe (the slope). An approximate fit to the data of figure 10 is

$$(1/2\pi)a_iD^2/\nu = f_oD^2/\nu \approx 5.46 + 0.11\ (Re - Re_{cr}). \qquad (5.13)$$

As the amplitude saturates to (5.10), the frequency shifts and asymptotes to a value f_s given by

$$f_sD^2/\nu = a_{io}D^2/2\pi\nu + (1/2\pi)\ [d(a_iD^2/\nu)/dRe - (c_{io}/c_{ro})\ d(a_rD^2/\nu)/\ dRe]\ (Re - Re_{cr}) - (1/2\pi c_{ro})\ d(a_rD^2/\nu)/dRe\ (Re - Re_{cr})^2\ dc_i/dRe, \qquad (5.14)$$

where c_i has been expanded in terms of $(Re - Re_{cr})$, and $c_{io} = c_i(Re_{cr})$. The last term in (5.14) depends quadratically on the difference Reynolds number and can be neglected on the basis of the well-known empirical finding (equation (4.2)) that the frequency f_s in the saturation state varies linearly with $(Re - Re_{cr})$. The condition for this, analogous to (5.9), is that

$$c_{io} >> dc_i/dRe\ (Re - Re_{cr}). \qquad (5.15)$$

Dropping the nonlinear term in (5.13) we write

$$f_sD^2/\nu = a_{io}D^2/2\pi\nu + (1/2\pi)[d(a_iD^2/\nu)/dRe - (c_{io}/c_{ro})d(a_rD^2/\nu)/dRe](Re - Re_{cr}). \qquad (5.16)$$

Experimentally, we find that

$$f_sD^2/\nu \approx 5.46 + 0.21\ (Re - Re_{cr}). \qquad (5.17)$$

for the aspect ratio 60 (figure 11) and beyond. Figure 11 shows data at two other two aspect ratios also, which will be useful in §5.4. The shift in frequency, $\Delta f = f_s - f_o$, is given by the difference between (5.17) and (5.13) to be

$$\Delta fD^2/\nu \approx 0.1(Re - Re_{cr}). \qquad (5.18a)$$

As seen from independent measurements given in the inset to figure 11, the fit (5.18a) describes the frequency increment quite well. The exact combination of constants responsible for the frequency shift becomes transparent when we write, from (5.12) and (5.17), that

$$\Delta f D^2/\nu = -[c_{io}/(2\pi c_{ro})\, d(a_r D^2/\nu)/dRe]\, (Re - Re_{cr}). \qquad (5.18b)$$

In summary, comparing (5.13) with (5.12), and (5.17) with (5.16), we obtain the following three further results:

$$a)\ a_{io} D^2/2\pi\nu \approx 5.46, \qquad (5.19a)$$

$$b)\ d(a_i D^2/\nu)/dRe \approx 0.7, \qquad (5.19b)$$

and

$$c)\ (c_{io}/c_{ro}) \approx -3.1. \qquad (5.19c)$$

We emphasize that all these results are independent of the spatial position in the wake.

Finally, if we can estimate $c_{ro}(x)$ from saturation amplitude measurements (see equation (5.10)), $c_{io}(x)$ can be calculated from (5.18c). Equivalently, since the slope of the line in figure 9 is $d(fD^2/\nu)/du_o^2 = -c_{io}D^2/(2\pi\nu)$, $c_{io}(x)$ can be determined directly; (5.18c) then yields $c_{ro}(x)$.

5.3 Frequency changes during decay

The analogue of the onset frequency in the subcritical regime is the frequency observed in the limit of zero amplitude, that is when the externally excited oscillations have decayed to zero amplitude. Since one can in principle excite oscillations at any frequency in the subcritical regime, frequency changes during decay can be positive or negative in general. The data obtained by the method (c) mentioned in §4.2 show that the oscillation frequency decreases during decay. Those obtained by exciting wake oscillations, mechanically or acoustically, at the special value given by the backward extrapolation of the saturation frequency (4.2), confirmed that a frequency *increase* accompanied the decay. From such studies, we conclude that the frequency of oscillations always approaches (5.13) during decay, from below if it is

initially lower and from above if it is initially higher; this leads to the view that the wake in its subcritical state prefers to set up oscillations given by (5.13). We merely note here that (5.13) corresponds to the backward extrapolation of the onset frequency in the supercritical regime, and leave a more detailed interpretation to §5.7 and §7.

5.4 A further simplification

According to the analysis so far, the five constants da_r/dRe, a_{io}, da_i/dRe, c_{ro} and c_{io} specify the evolution of the frequency and amplitude of oscillations in the periodic state. It is worth repeating that the first three constants, and the ratio between the fourth and the fifth, are independent of the spatial position. A simple observation, which follows from a comparison of growth rate and saturation frequency data, reduces the number of constants by one. We measured growth rates as well as the saturation (that is, the vortex shedding) frequency at four different aspect ratios, and found that the slopes $d(a_rD^2/\nu)/dRe$ and $d(f_sD^2/\nu)/dRe$ are nearly equal to each other even though the individual slopes do vary with aspect ratio. (See, for example, figure 11 for the latter quantity.) Although measurements at the smallest aspect ratio of 5 were not very clean because of several operational difficulties associated with small aspect ratio cylinders – here, the reduction in the aspect ratio was achieved by bringing the end plates closer – the conclusion regarding the slopes was borne out to within the experimental accuracy (see table 2). The conclusion then is that

$$(1/2\pi)\, d(a_iD^2/\nu)/dRe \approx (c_{io}/2\pi c_{ro} + 1)\, d(a_rD^2/\nu)/dRe, \qquad (5.20)$$

which reduces the number of independent constants to four.

Returning now to the observation in §4.1 that the dominant frequency on the wake centerline is twice that in the shear layer, we note that a simple consequence of the equality between da_r/dRe and df_s/dRe is that the centerline frequency must grow at twice the rate of the vortex shedding frequency. This has been observed to be true both experimentally and in the computation described in II. It has since also been confirmed by Hannemann & Oertel (1988) in the wake of a flat plate.

5.5 Summary of Landau-Stuart constants

For the large aspect ratio (L/D ≈ 60 and above), we have:

$$a_r D^2/\nu \approx 0.20\,(Re - Re_{cr}) \quad (5.21a)$$

$$a_i D^2/\nu \approx 34.3 + 0.7\,(Re - Re_{cr}) \quad (5.21b)$$

$$dc_r/dRe \approx dc_i/dRe \approx 0 \quad (5.21c)$$

$$c_{io}/c_{ro} \approx -3. \quad (5.21d)$$

These results are independent of the flow Reynolds number in the neighbourhood of Re_{cr} and the space coordinate. If the value of c_{ro} inferred from the saturation amplitude data of figure 8 can be considered representative, we obtain:

$$c_{ro} D^2/\nu \approx 0.024, \text{ and } c_{io} D^2/\nu \approx -0.06. \quad (5.22)$$

5.6 Hopf bifurcation

Writing again $\mathbf{u}$ as $u_o \exp(i\phi(t))$, noting that $u_o = \exp(a_r t)$, and, from (5.3) that $d\phi/dt = a_i$ for linear amplitudes, we have:

$$\begin{bmatrix} u_r' \\ u_i' \end{bmatrix} = \begin{bmatrix} a_r & -a_i \\ a_i & a_r \end{bmatrix} \begin{bmatrix} u_r \\ u_i \end{bmatrix}$$

The square matrix in the above equation gives A in equation (2.1). The eigenvalues of this matrix are easily shown to be $a_r \pm (\sqrt{-1})a_i$, both known from measurement to be independent of the spatial coordinate as well as the Reynolds number (in a finite neighbourhood of Re_{cr}). From this, we can now determine how the eigenvalues journey in the complex plane as the Reynolds number increases from below Re_{cr} to above Re_{cr}. This is done in figure 12. Clearly, the eigenvalues cross the imaginary axis at Re_{cr} (which by definition corresponds to $a_r = 0$). Also, the speed at which the real part of the eigenvalues crosses the imaginary axis is given by $da_r/dRe = 0.2\nu/D^2$.

5.7 Comparison with previous measurements

As already noted, the present measurements overlap with those reported by Mathis et al. (1984), and its sequel by Provansal et al. (1987). Here, we highlight the similarities and differences between the present measurements and these two sets of data.

Mathis et al. were the first to study experimentally the bifurcation characteristics of the vortex shedding process. Their measurements of the normal velocity component were made on the wake centerline at x/D = 5 for a cylinder of aspect ratio 60, and concerned exclusively the saturation state. They established the proportionality between the saturation amplitude and the square root of the difference Reynolds number on the one hand, and a similar proportionality between the saturation frequency and the Reynolds number. They also estimated the critical Reynolds number to be 50. Provansal et al. reported more detailed measurements for cylinders of several aspect ratios. Of primary interest here are their transient measurements accompanying an impulse disturbance created by striking an elastic diaphragm upstream of the test section. By such measurements, Provansal et al. determined the constant a_r and established the linear relationship between a_r and Re (equation (5.20a)) for $(Re - Re_{cr})$. It should be noted that the measurements of Mathis et al. and Provansal et al. did not include any spatial variation of oscillations; this has been one of our concerns. A comparison of the various Landau constants from the two related studies is given in table 3.

It is clear that the agreement in the first three quantities is excellent, showing that the streamwise and normal velocity fluctuations both develop similarly. In particular, the constancy of the quantity $d(a_r D^2/\nu)/dRe$ in both sets of data holds over a sizeable neighbourhood of $Re-Re_{cr}$. One difference is in the ratio c_i/c_r: It is nonzero in the present experiments whereas Provansal et al. conclude that c_i is essentially zero. (Perhaps coincidentally, their c_r is quite close to the value given in §5.5.) Noting that c_i is related to the nonlinear effect producing a frequency shift during the growth phase of the disturbance, the present results, unlike those of Provansal et al., suggest a sizeable frequency shift; this has already been discussed in §5.2. That there is such a frequency shift was noted by Thomas &

Szewczyk (1969); Hannemann (1987) and Hannemann & Oertel (1988) have also carefully documented it in their numerical investigation of the impulsively started flow past a flat plate. We believe that the reason why Provansal et al. did not detect substantial shift is that their experiments involved an increase in Reynolds number from one supercritical value to another in close vicinity, and not from the subcritical to the supercritical as in our experiments.

But one could look at the problem in another way. As already remarked, we found that the preferred frequency in the subcritical regime lies on a backward extrapolation of the onset frequency curve. Since the asymptotically preferred frequency in the supercritical regime is the saturation frequency given by (5.17), it is clear that this implies a discontinuity in slopes of the preferred frequencies as we cross the critical Reynolds number. A replot of the data of Provansal et al.'s figure 8 on their figure 11 does in fact confirm this discontinuity. In private correspondence approximately two years ago, Provansal and Boyer have kindly confirmed that the data of Mathis (1983) can be interpreted to give a value for the ratio c_i/c_r of order unity, in qualitative agreement with the present results.

6. Is the wake absolutely unstable ?

6.1 The background

We have thus shown that the onset of vortex shedding occurs strictly according to the Hopf bifurcation. We have also shown that, in a certain non-trivial neighborhood of the critical Reynolds number, the supercritical state is described by the Landau-Stuart equation (5.1). One important finding of this work is that the spatial nature of the problem appears only in a secondary role, namely in the dependence of the constants **c**. This may at first appear surprising because intuition suggests that the problem must be spatial in character. The Landau-Stuart equation in which only the constants **c** are spatially dependent cannot in principle be completely self-consistent, but apparently it represents a good approximation to reality. Unlike most other familiar instabilities, such as in isothermal constant density jets and boundary layers, the onset of the periodic state is strictly *via* a Hopf bifurcation.

We recall from §1 the suggestion that the wake instability giving rise to vortex shedding

is of the absolute type. We recapitulate the concept of absolute instability briefly – for a more detailed discussion see, for example, Huerre & Monkewitz (1985) – and describe measurements which shed light on the suggestion. The concepts of absolute and convective instability develop quite naturally from an analysis in which an impulse-type disturbance is introduced into an infinitely parallel shear flow (the basic state) and allowed to develop in both space and time. If the shear flow is unstable it will contain amplified waves travelling at their group velocity, and the evolution of these amplified wavepackets determines the nature of the flow instability. A convective instability results if a wavepacket introduced at a spatial position x_0 and time t_0 has a positive group velocity when amplified, so that it gets convected away with the flow, leaving the basic state locally undisturbed for large times. If the amplified wave packet has zero group velocity, it grows locally and will eventually dominate the flow development; the nonlinearities of the system prevent the amplitude of the disturbance from becoming unbounded and a saturation amplitude is reached. In contrast to a convectively unstable flow where the amplified disturbance has contributions from all wavenumbers growing as they convect, an absolutely unstable flow is dominated by a pure frequency instability. We already showed in §1 that the wake oscillations extremely sharp spectral peaks. Prompted primarily by this observation, we have studied the vortex shedding process in the context of the absolute stability characteristics discussed above in qualitative terms. Related information can be found in II.

An absolutely unstable flow is insensitive to the amplitude of the initial disturbance since this amplitude will only determine how long it takes for the disturbance to grow but will not affect the *rate* at which it grows or the saturation amplitude that is eventually reached. But, an absolutely unstable flow will show sensitivity to small configurational changes since it is dominated by a local instability. Hence an external device which *locally* alters the basic state (mean velocity profile) may profoundly affect the nature of instability. In contrast, a convectively unstable flow will be sensitive to initial disturbance amplitude; the disturbance growth being an integrated effect along the path of propagation of the disturbance, local alterations of the basic state will have little effect on the final state. In II, we have discussed

the dramatic effect that a simple scheme of altering the mean velocity profile has on wake stability: The placement of a second, much smaller, cylinder in an appropriate position in the wake severely alters and even completely suppresses vortex shedding in a certain non-trivial range of Reynolds numbers above the critical.

A systematic study of the insensitivity of vortex shedding to the initial disturbance level has not been attempted before. Below, we give some results. We chose to vary the initial disturbance amplitude either by varying the external acoustic excitation or the freestream turbulence level, and studied the effects on vortex shedding – in terms of temporal growth rates, saturation amplitudes and the critical Reynolds number.

6.2 The insensitivity of the saturation amplitude to excitation levels

The vortex shedding wake was acoustically excited using the experimental set-up shown in figure 13. The acoustic excitation produced by the 10 cm diameter speaker was monitored by a Bruel & Kjaer (type 1613) acoustic pressure meter (type 4165 microphone) placed in the opposite test section wall. The excitation frequencies used were much lower than those of possible standing wave modes in the wind tunnel test section. The frequency of acoustic excitation was set at the natural shedding frequency for $Re > Re_{cr}$ (= 43 for this particular flow). Below Re_{cr} the vortex shedding was artificially excited at the frequency producing the largest wake response for a given acoustic excitation level. This frequency has a Strouhal number $St = fD/U_0 = 0.1$, coincident with the spatially most amplified frequency of Nishioka & Sato (1978). A hot-wire placed at an x/D = 10 in the shear layer measured the streamwise velocity component. As discussed previously, one would expect an absolutely unstable flow to yield a saturation amplitude which is independent of the initial disturbance amplitude. In figure 14, which shows the saturation amplitude *vs* acoustic excitation level, we see that this is indeed the case for $Re > 43$, the wake response being flat to excitation levels up to 25 dB above background noise levels. In sharp contrast, the wake response for $27 < Re < 40$ shows an approximately linear response to acoustic excitation level. This suggests that the flow over a circular cylinder for Reynolds number below critical is indeed convectively

unstable. It should be noted that it was extremely difficult to artificially excite vortex shedding below Re $\simeq$ 25 suggesting that the flow becomes completely stable at these low Reynolds numbers (see also § 4.2).

6.3. The insensitivity of temporal growth rates and the critical Reynolds number to the background noise level

This question was studied in the facility described in §3.1.1. The cylinder aspect ratio was approximately 60. The freestream turbulence level was varied (in the range 0.03% to 0.19%) by placing additional screens approximately 100 diameters upstream of the shedding cylinder. Temporal growth rates were determined as before at x/D = 10. Figure 15 shows the temporal growth rates *vs* Reynolds number for three different freestream turbulence levels. Within the experimental scatter all the data collapse onto a single line with slope $da_r/dRe = 0.2\nu/D^2$, thus highlighting the insensitivity of temporal growth rates to freestream turbulence levels. Data from acoustic excitation produced the same result.

From the growth rate data, we have obtained the critical Reynolds numbers at different turbulence levels by determining where the least square fits to the growth rate data intersect the abscissa (corresponding to the zero growth rate condition); see figure 16. We note the insensitivity of critical Reynolds number as freestream turbulence level is varied, and contrast this with the well known sensitivity of Re_{cr} in the flat plate boundary layer (e.g., Schubauer & Skramstad 1947). Although we do not know of any specific analysis showing that the boundary layer is convectively unstable from the spatio-temporal point of view, circumstantial evidence seems to suggest that the instability there is of the convective type.

7. Summary

We have shown that the growth rates and the critical Reynolds number associated with the vortex shedding process are robust against background noise level. These characteristics are shared by absolutely unstable flows. The reason that we have been less than definitive in identifying wake instability leading to vortex shedding with absolute instability is that, as a

concept, the latter is strictly applicable to linear perturbations of the impulse type growing in space and time with zero group velocity in infinitely parallel flows (e.g. Briggs 1964). None of these criteria hold strictly in the present problem, especially because the characteristic wavelength of growing disturbances is not small compared to the extent of the flow domain participating in the global instability. It has been shown in II that this region is of the order of 4 diameters immediately behind the cylinder, where streamwise nonuniformities cannot be ignored. Yet, we believe that the general notion of absolute instability can have some value in describing the process. Perhaps it is more appropriate to think of the wake instability as of the global temporal type in which the instability mode extends in both transverse and streamwise directions; we particularly have in mind the numerical work of Jackson (1987). We have shown that the perturbation dynamics is governed by the Landau-Stuart equation where all the constants a and the ratio c_r/c_i are space-independent in a certain neighbourhood of the critical Reynolds number.

One of the interesting observations is that the onset frequency of the oscillations in the supercritical regime is given by (5.13), and that it shifts during evolution to the value given by (5.17). Further, all oscillation frequencies in the subcritical regime asymptote to (5.13) as they decay subsequent to the removal of the excitation source; the rate of decay is independent of the oscillation frequency. To understand its significance of these observations, we plot in figure 17 equations (5.13) and (5.17) and superimpose the data Nishioka & Sato (1978) corresponding to the spatially most amplified mode in the subcritical regime; also plotted is their saturation frequency data in the supercritical regime.There is good agreement in both the subcritical and supercritical regimes. It is clear that the extrapolation of their subcritical data to the supercritical regime is identical to the onset frequency given by (5.13). We assume that the extrapolation of the Nishioka-Sato line in the supercritical regime retains the same meaning, namely that it represents the spatially most amplified mode. It follows that in the subcritical regime all oscillations tend to favour the spatially most amplified mode, consistent with our earlier remark in §6 that there is a convective instability in the wake at Reynolds numbers above about 25. Oscillations in the supercritical regime begin at the spatially most

amplified frequency but soon change over to the temporally most amplified value because the latter is so overwhelmingly large; the change in frequency is the essential manifestation of nonlinearity. Below a Reynolds number of 25, the wake appears to be completely stable.

The primary factor that sets wake instability apart from that in many other familiar fluid flows, such as constant density isothermal jets and boundary layers, is that a finite region participates as a whole in the evolution process. In this sense vortex shedding in wakes shares some important characteristics of dynamical systems. As already remarked, some consequences of this feature have been explored in Sreenivasan (1985), Olinger & Sreenivasan (1988a,b), and Chhabra et al. (1989), and more work is in progress. It is pertinent to note that similar phenomenon occurs in variable density jets (Kyle 1986, Sreenivasan, Raghu & Kyle 1989) and heated jets (Bechart, Lehmann, Barsikov & Monkewitz 1988).

Acknowledgements

We are thankful to Professors Boyer and Provansal for a useful correspondence. The research was supported by grants from Air Force Office of Scientific Research and by the National Science Foundation.

References

Bechart, D.W., Lehmann, B., Barsikow, B. & Monkewitz, P.A. 1988 Heated jets are different, Abstract BD4, Bull. Amer. Phy. Soc. **33**, 2237.

Berger, E. 1964 Unterdrückung der laminaren Wirbelströmung und des turbulezeinsatzes der Kármánschen Wirbelstrasse im nachlauf eines schwingenden Zylindersbei kleinen Reynoldszahlen. In Jahrbuch der Wissenschaftlichen Gesellschaft für Luft-und-Raumfahrt, pp.164-172.

Briggs, R.J. 1964 Electron-stream interaction with plasmas. Research Monograph. no. 29, Cambridge, Mass.M.I.T. Press.

Chhabra, A., Olinger, D. & Sreenivasan, K.R. 1989 The onset of chaos in the wake of an oscillating cylinder: theory and experiment. Accepted for presentation in the Forum on Chaotic Dynamics in Fluid Mechanics, ASME meeting, July 1989.

Cimbala, J.M., Nagib, H.M. & Roshko, A. 1988 Large structure in the far wakes of two-dimensional bluff bodies. J. Fluid Mech. **190**, 265-298.

Guckenheimer, J. & Holmes, P. 1983 Nonlinear oscillations, dynamical systems and bifurcations of vector fields, Springer (Applied Mathematical Sciences Series, Vol. 42).

Hannemann, K. 1987 Numerische Simulation und stabilitätstheoretische Untersuchung des absolut und konvektiv instabilen Nachlaufs. Ph.D. Thesis, Universität Karlsruhe.

Hannemann, K. & Oertel, H. 1988 Numerical simulation of the absolutely and convectively unstable wakes. J. Fluid Mech. (in print)

Huerre, P. 1985 Spatio-temporal instabilities in closed and open flows. Proc. Int. Workshop on Instabilities and Non-Equilibrium Structures, Valparaiso, Chile 16-21 Dec.

Huerre, P. and Monkewitz, P.A. 1985 Absolute and convective instabilities in free shear layers, J. Fluid Mech. **159**, 151-168.

Jackson, C.P. 1987 A finite-element study of the onset of vortex shedding in flow past variously shaped bodies. J. Fluid Mech. **182**, 23-45.

Jensen, M.H., Kadanoff, L.P., Libchaber, A., Procaccia, I. & Stavans, J. 1985 Phys. Rev. Lett. **55**, 2789-91.

Joseph, D.D. 1976 Stability of Fluid motion I. Springer Tract of Natural Philosophy, Vol. 28.

Koch, W. 1985 Local insability characteristics and frequency determination of self-excited wake flows. J. Sound Vib. **99**, 53-83.

Kovasznay, L.S.G. 1949 Hot-wire investigation of the wake behind cylinders at low Reynolds numbers, Proc. Roy. Soc. London A **198**, 174-190.

Kyle, D. 1986 Absolute instability in variable jets. Dept. Mech. Eng., Yale University, Rep. 86-FM6.

Landau, L.D. and Lifshitz, E.M. 1959 Fluid Mechanics-Vol. 6 Course of theoretical physics, Pergamon Press London.

Libchaber, A. & Maurer, J. 1981 A Rayleigh-Benard experiment: helium in a small box. In Nonlinear Phenomena at Phase Transitions and Instabilities (ed. T. Riste), pp 259-86. NATO Report.

Mair, W.A. & Maull, D.J. 1971 Bluff bodies and vortex shedding - a report of Euromech 17. J. Fluid Mech. **45**, 209-224.

Mathis, C. 1983 Propriétés des composantes de vitesse trasverses dans l'écoulement de Bénard-von Kármán aux faibles nombres de Reynolds. Thesis Université Ais-Marseille.

Mathis, C., Provansal, M. and Boyer, L. 1984 The Benard-von Kármán instability: an experimental study near the threshold, J. de Phys. Lett. **45**, L483-491.

Monkewitz, P.A. 1988 The absolute and convective nature of instability in two-dimensional wakes at low Reynolds numbers. Phys. Fluids **31**, 999-1006.

Monkewitz, P.A. & Nguyen, L.N. 1987 Absolute instability in the near-wake of two-dimensional bluff bodies. J. Fluids and Structures **1**, 165-184.

Nishioka, M. and Sato, H. 1974 Measurements of velocity distributions in the wake of a circular cylinder at low Reynolds numbers, J. Fluid Mech. **65**, 97-112.

Nishioka, M. and Sato, H. 1978 Mechanism of determination of the shedding frequency of vortices behind a cylinder at low Reynolds numbers, J. Fluid Mech. **89**, *49-60*.

Olinger, D.J. & Sreenivasan, K.R. 1988a Nonlinear dynamics of the wake of an oscillating cylinder, Phys. Rev. Lett. **60**, 797-800.

Olinger, D.J. & Sreenivasan, K.R. 1988b Low Reynolds number dynamics in the wake of an oscillating cylinder. In: Proc. ASME Int. Symp. Flow Induced Vibrations and Noise, pp. xx-yy.

Provansal, M., Mathis, C. and Boyer, L. 1986 Benard-von Karman instability: Transient and forced regimes, J. Fluid Mech.**182**, 1-22.

Roshko, A. 1954 On the development of turbulent wakes from vortex streets, NACA Rep. 1191.

Schubauer, G.B. & Skramstad, H.K. 1947 Laminar boundary layer oscillations and stability of laminar flow. J. Aero. Sci. **14**, 69-78.

Sreenivasan, K.R. 1985 Transition and turbulence in fluid flows and low-dimensional chaos. In Frontiers in Fluid Mechanics (eds. Davis, S.H. and Lumley, J.L.), Springer-Verlag, pp.41-67.

Sreenivasan, K.R. & Ramshankar, R. 1986 Transition intermittency in open flows, and intermittency routes to chaos, Physica 23D, 246-258.

Sreenivasan, K.R., Raghu, S. & Kyle, D. 1988 Absolute instability in variable density jets. Experiments in Fluids (in press).

Sreenivasan, K.R., Strykowski, P.J. & Olinger, D. 1986 Hopf bifurcation, Landau equation and vortex shedding behind circular cylinders. In: ASME Forum on Unsteady Separation, FED-Vol.52, pp.1-14.

Stansby, P.K. 1974 The effects of end plates on the base pressure coefficient of a circular cylinder, Aero. Journal **78**, 36-37.

Strykowski, P.J. 1986 The control of absolutely and convectively unstable shear flows, Ph. D. thesis, Yale University.

Strykowski, P.J. and Sreenivasan, K.R. 1985 The control of transitional flows, AIAA Shear Flow Control Conference, Boulder Colorado, March 12-14.

Strykowski, P.J. and Sreenivasan, K.R. 1988 On the formation and suppression of vortex 'shedding' at low Reynolds numbers. Submitted to J. Fluid Mech. (referred to as II)

Stuart, J.T. 1958 On the nonlinear mechanics of hydrodynamic stability. J. Fluid Mech. **4**, 1-21.

Stuart, J.T. 1960 On the nonlinear mechanics of wave disturbances in stable and unstable parallel flows. Part 1. The basic behaviour in plane Poiseuille flow. J. Fluid Mech. **9**, 353-370.

Taneda, S. 1963 The stability of two-dimansional laminar wakes at low Reynolds numbers. J. Phy. Soc. Japan, **18**, 288-296.

Thoman, D.C & Szewczyk, A.A. 1969 Time-dependent viscous flow over a circular cylinder. Phys. Fluids. Suppl. **12**, II-76.

Table 1

Nomenclature:

D ... Cylinder diameter.
L ... Cylinder length between end plates.
H ... Height of test section normal to cylinder axis and freestream.

Low Turbulence Wind Tunnel

D (cm)	L/D	H/D
0.08	60	60

Single Contraction Wind Tunnel

D (cm)	L/D	H/D
0.15	60	72
0.15	27	72
0.15	14	72
0.32	60	33
0.18	60	58

Table 2

Aspect Ratio	$d(f_s D^2/\nu)/dRe$	$d(a_r D^2/\nu)/dRe$
60	0.21	0.20
27	0.20	0.19
14	0.17	0.17
5	0.17	0.17

Table 3

quantity	Provansal et al.	Present
Re_{cr}	47	46 (both for L/D = oo)
$d(a_r D^2/\nu)/dRe$	0.2	0.2
$a_{io} D^2/(2\pi\nu)$	5.7 (L/D =66) 4.6 (L/D = 33)	5.46 (L/D = 60)
c_{io}/c_{ro}	≈ 0 (see text)	≈ -3

Figure captions

Fig. 1. Normalized power spectral density of the streamwise velocity component in the wake (x/D = 10, y/D = 1) at a Reynolds number of 48. Here, x is the streamwise distance measured from the cylinder axis, and y is the coordinate normal to it; D is the cylinder diameter. The power P is plotted on logarithmic scale to base 10. The peak marked f_1 at about 590 Hz. corresponds to the vortex shedding frequency, and the subsequent strong peaks above the noise level are the harmonics of f_1. The strongest peak is about seven orders of magnitude above the noise level, and all peaks are extremely sharp.

Fig. 2. Hopf bifurcation: A schematic

Fig. 3. Simultaneous records of the mean and fluctuating velocities. The flow Reynolds number, Re, was increased from 43 to 49. As will be determined later, the critical Reynolds number, Re_{cr}, is 46. Trace (a) was low pass filtered below 30 Hz. and trace (b) was high pass filtered above 30 Hz. The aspect ratio, L/D, of the cylinder was 60.

Fig. 4. Trace (a) is the amplitude of the fluctuating velocity. The logarithm of the amplitude envelope is plotted in (b). The Reynolds number is 49. The growth rate $a_r = 4.5$ sec^{-1}.

Fig. 5. Fluctuating velocity response, measured during decay. The flow Reynolds number is reduced from 50 to 44. Signal measured at x/D = 10 in the shear layer. $Re_{cr} = 46$, L/D = 60.

Fig. 6. Growth and decay rates. ○, turbulence level = 0.09%. □, decay rates for acoustically excited oscillations; △, decay rates for oscillations excited by cylinder oscillations, St = 0.1; ◇, same as in the previous case, oscillation frequency given by (4.2). The inset shows growth rate measurements made at different streamwise positions at Re = 60.

Fig. 7. Amplification and decay rate measurements for an aspect ratio of 60; only amplification rates have been measured for aspect ratios of 27 and 14. ○, aspect ratio 60; ▽, 27; □, 14.

Fig. 8. The saturation amplitude at x/D = 5, y/D = 0.5 in the wake of the cylinder.

Measurements using the LDV.

Fig. 9. Relationship between frequency of oscillations and their amplitude. The upper curve corresponds to decay at Re = 30 and the lower curve to amplification at Re = 62. The intercept determines the onset frequency $a_i D^2/2\pi\nu$. L/D = 60.

Fig. 10. The dependence of the onset frequency $a_i/2\pi$ on the difference Reynolds number $Re - Re_{cr}$. These data were compiled from data similar to figure 9 for various Reynolds numbers.

Fig. 11. The variation of the saturation frequency with Reynolds number for three different aspect ratios. O , aspect ratio 60; ∇, 27; □, 14.

Fig. 12. As the Reynolds number increases from below Re_{cr} to above Re_{cr}, the complex conjugate eigenvalues of the matrix A in (2.1) move from the left half of the plane to the right at a speed given by $d(a_r D^2/\nu)/dRe$.

Fig. 13. Schematic of apparatus for the the acoustic excitation work; not to scale.

Fig. 14. Wake saturation amplitude *vs* external acoustic excitation. Both axes are in logarithmic scales to base 10. Hot wire position x/D = 10, y/D = 1.O, Re = 27; □ , Re = 30; Δ , Re = 36; ◆ , Re = 46; ■ , Re = 51; ● , Re = 61.

Fig. 15. Growth rates at different freestream turbulence levels. , turbulence level of 0.09%; , 0.16%; , 0.19%. The continuous line corresponds to equations (4.3), and is a good fit to data obtained at a turbulence level of 0.03%.

Fig. 16. Critical Reynolds numbers as a function of the freestream turbulence level

Fig. 17. Dimensionless onset and saturation frequencies as a function of the difference Reynolds number. The onset frequency is given by (5.13) and shown dashed. The continuous line is the saturation frequency given by (5.17). The symbols are data from Nishioka & Sato. The subcritical data (◆) for the spatially most amplified mode are taken from their figure 8b. The supercritical data are for the saturation oscillations, taken from their figure 10.

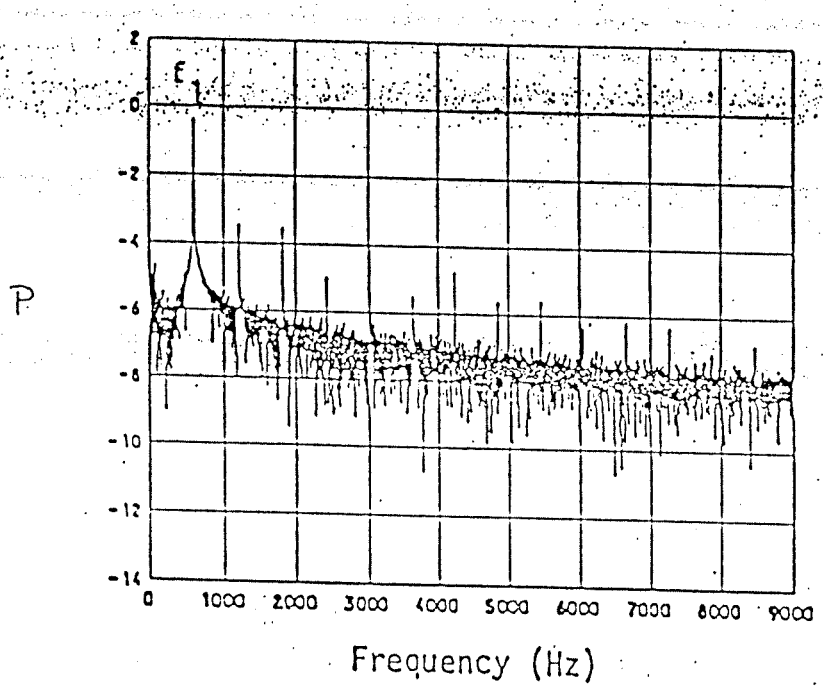

Fig. 1. Normalized power spectral density of the streamwise velocity component in the wake (x/D = 10, y/D = 1) at a Reynolds number of 48. Here, x is the streamwise distance measured from the cylinder axis, and y is the coordinate normal to it; D is the cylinder diameter. The power P is plotted on logarithmic scale to base 10. The peak marked f_1 at about 590 Hz. corresponds to the vortex shedding frequency, and the subsequent strong peaks above the noise level are the harmonics of f_1. The strongest peak is about seven orders of magnitude above the noise level, and all peaks are extremely sharp.

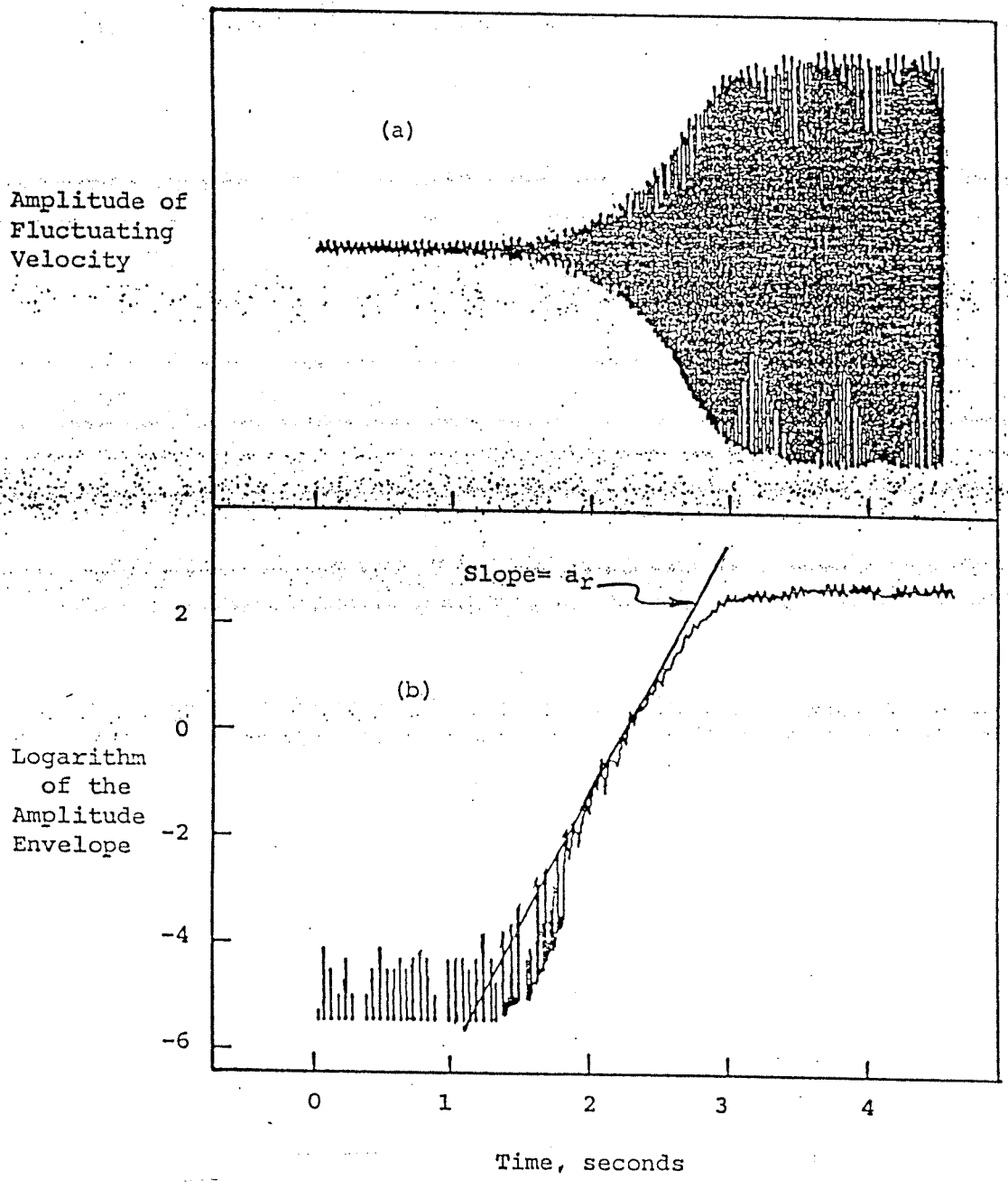

Fig. 4. Trace (a) is the amplitude of the fluctuating velocity. The logarithm of the amplitude envelope is plotted in (b). The Reynolds number is 49. The growth rate $a_r = 4.5$ sec^{-1}.

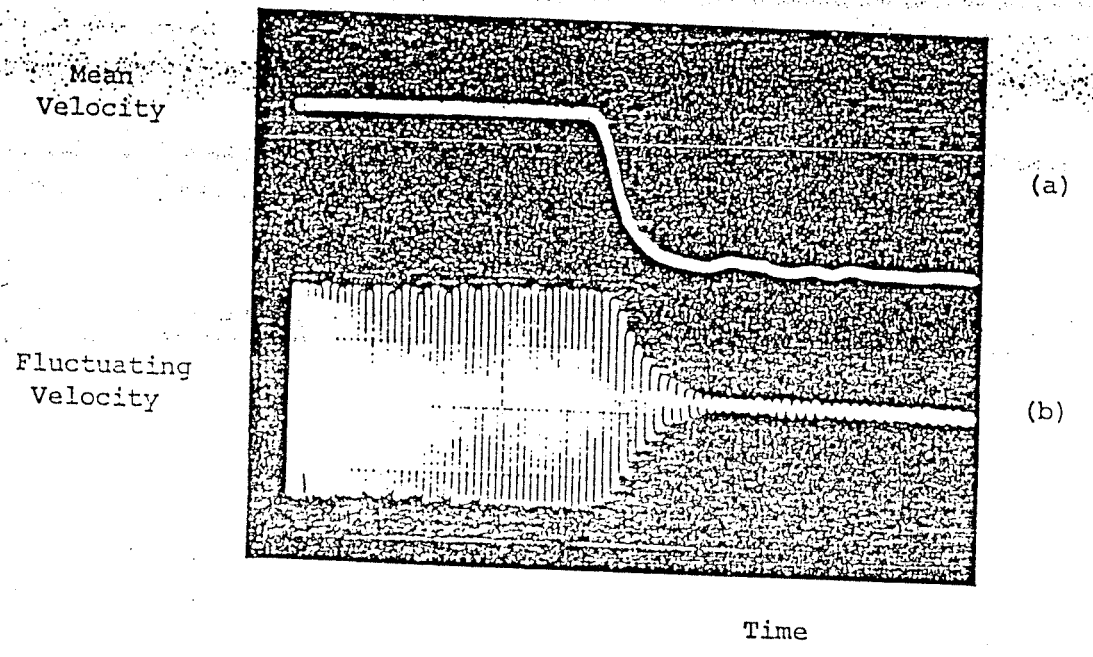

Fig. 5. Fluctuating velocity response, measured during decay. The flow Reynolds number is reduced from 50 to 44. Signal measured at x/D = 10 in the shear layer. Re_{cr} = 46, L/D = 60.

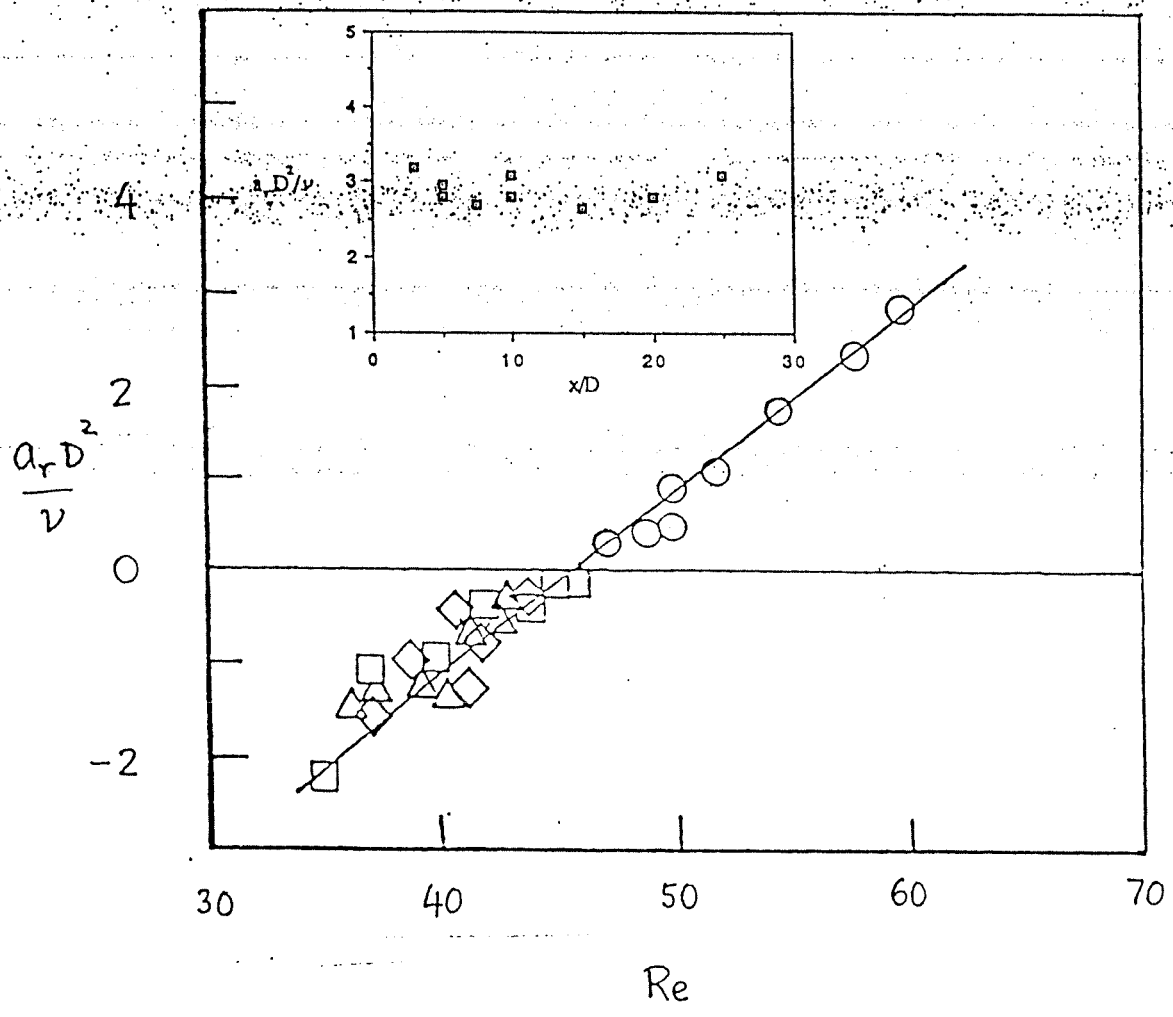

Fig. 6. Growth and decay rates. ○, turbulence level = 0.09%. □ , decay rates for acoustically excited oscillations; Δ , decay rates for oscillations excited by cylinder oscillations, St = 0.1; ◇ , same as in the previous case, oscillation frequency given by (4.2). The inset shows growth rate measurements made at different streamwise positions at Re = 60.

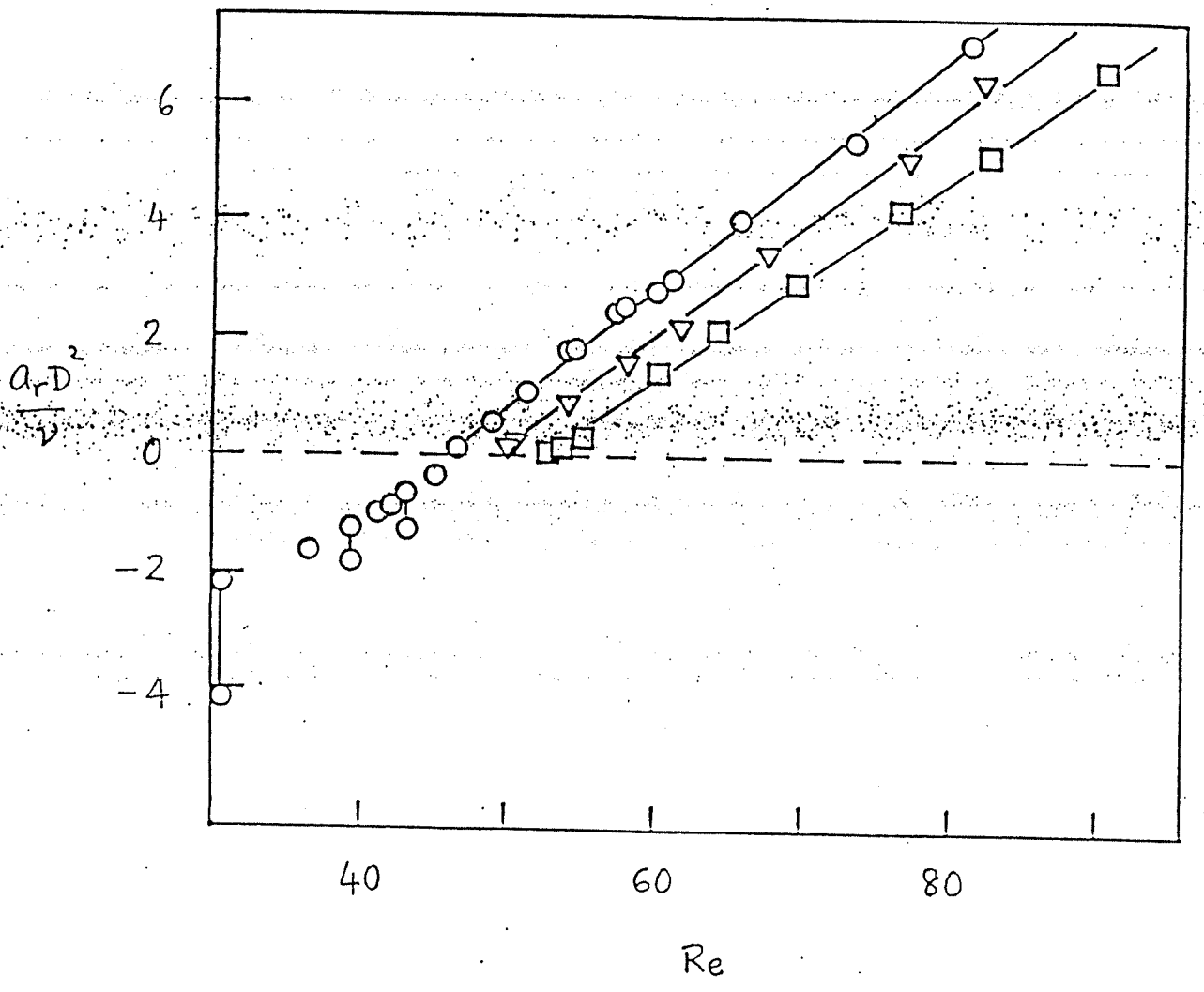

Fig. 7. Amplification and decay rate measurements for an aspect ratio of 60; only amplification rates have been measured for aspect ratios of 27 and 14. O, aspect ratio 60; ▽, 27; □, 14.

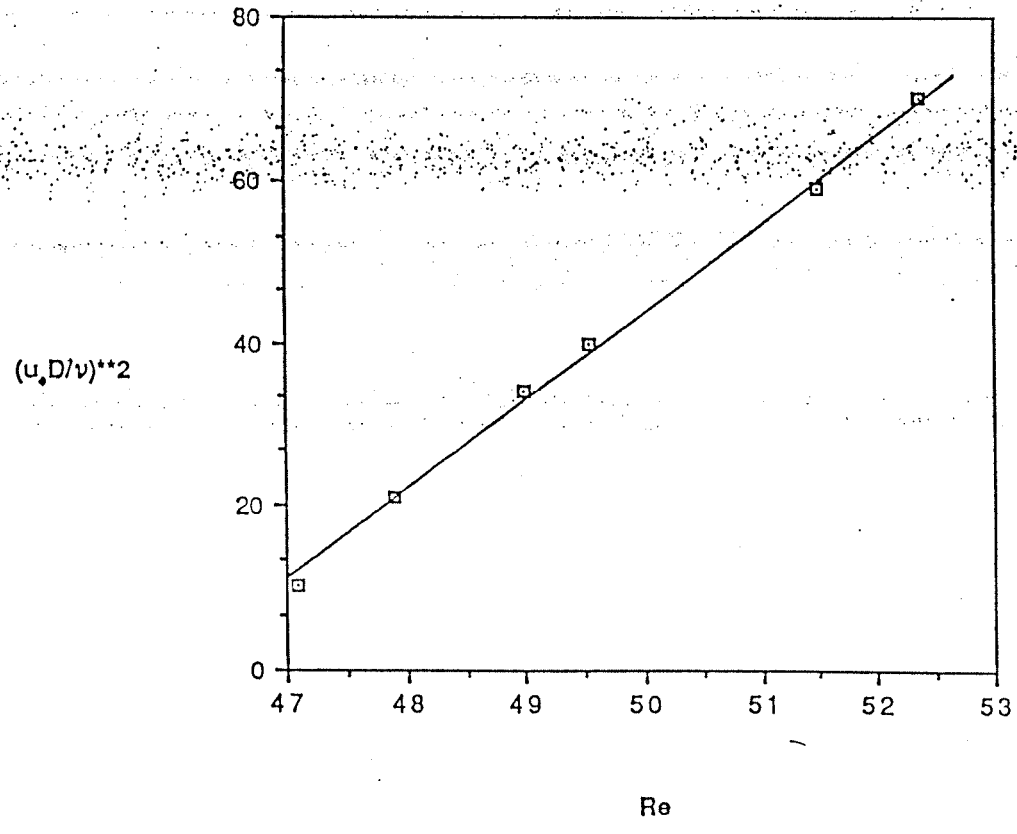

Fig. 8. The saturation amplitude at x/D = 5, y/D = 0.5 in the wake of the cylinder. Measurements using the LDV.

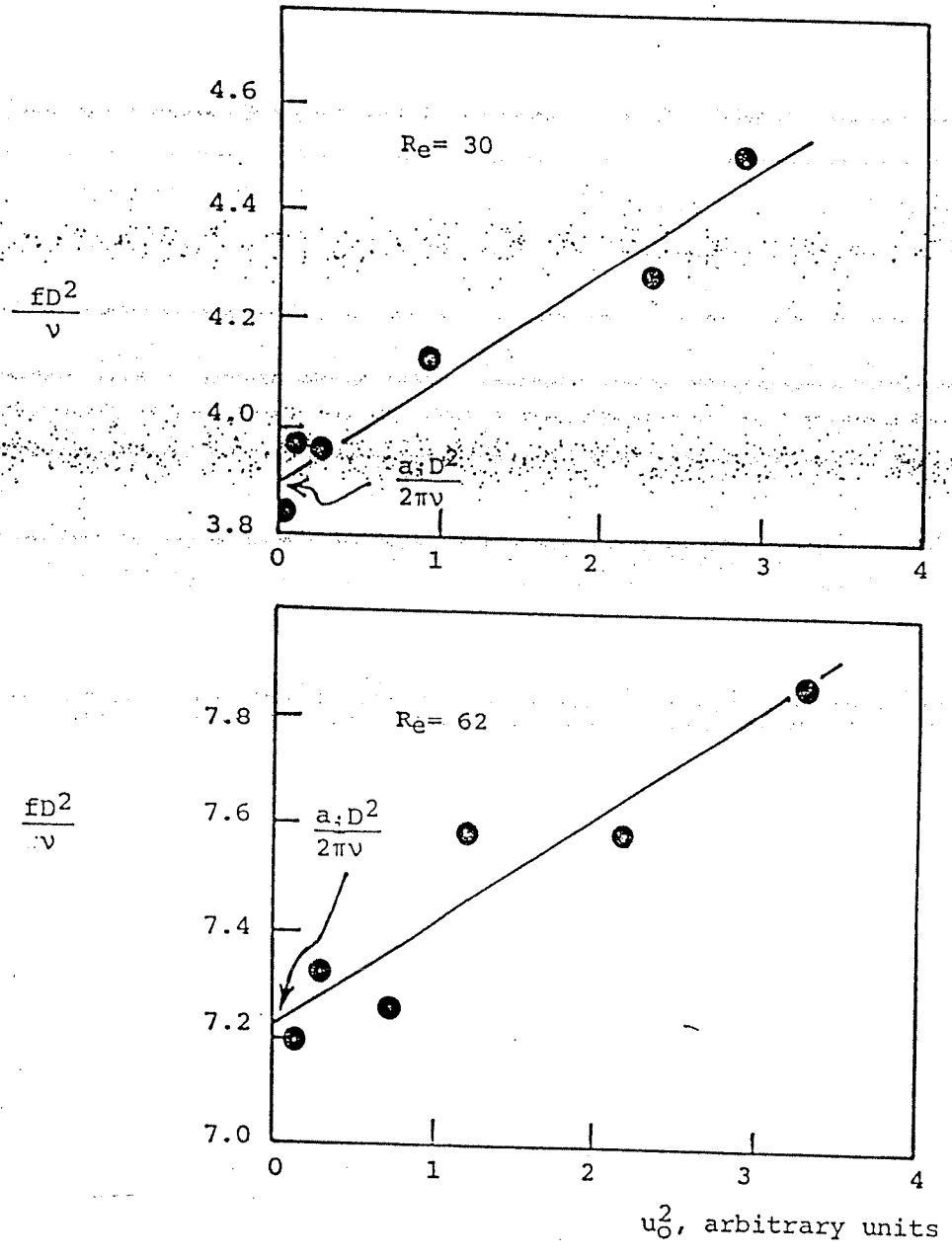

Fig. 9. Relationship between frequency of oscillations and their amplitude. The upper curve corresponds to decay at Re = 30 and the lower curve to amplification at Re = 62. The intercept determines the onset frequency $a_i D^2/2\pi\nu$. L/D = 60.

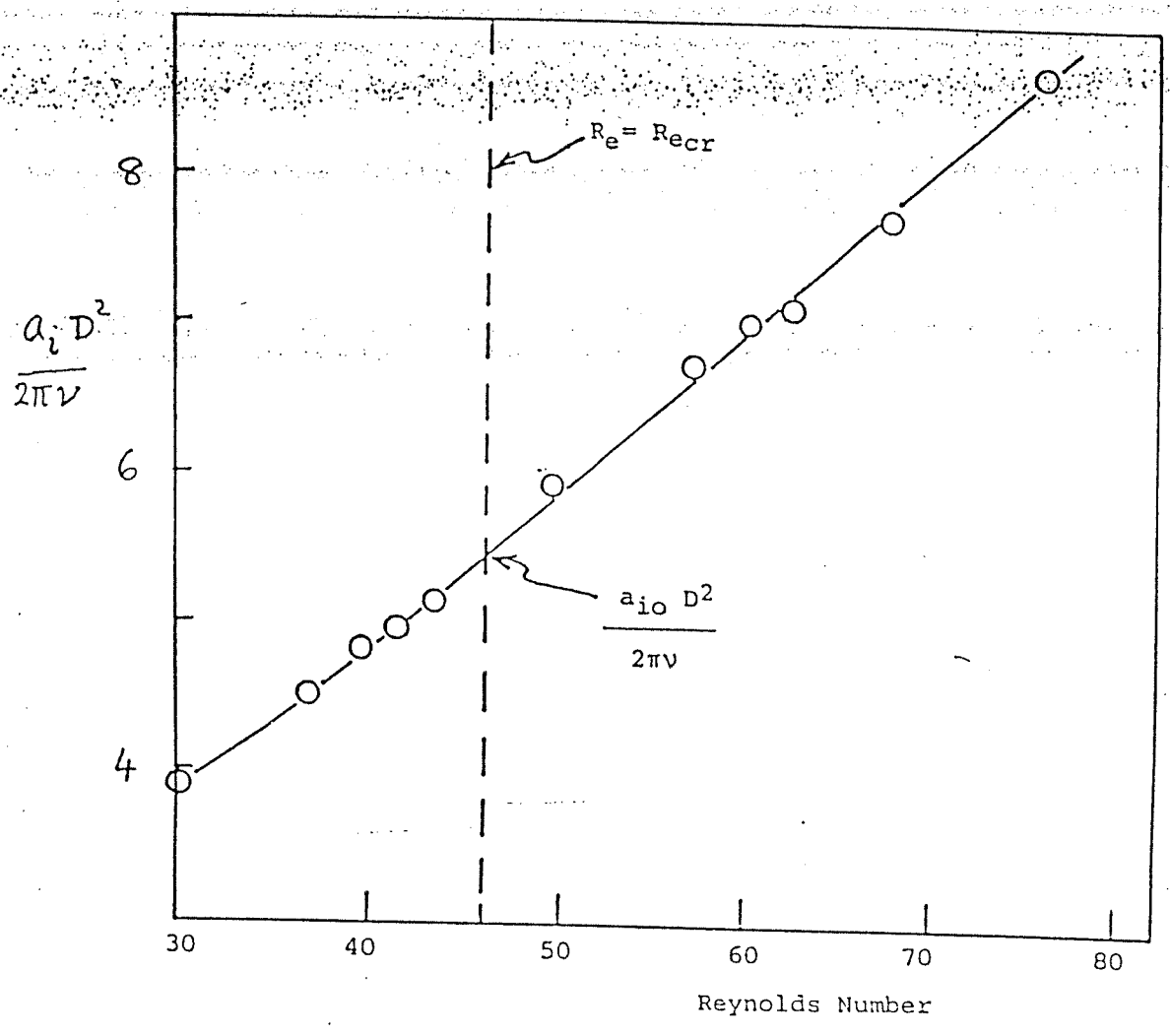

Fig. 10. The dependence of the onset frequency $a_i/2\pi$ on the difference Reynolds number $Re - Re_{cr}$. These data were compiled from data similar to figure 9 for various Reynolds numbers.

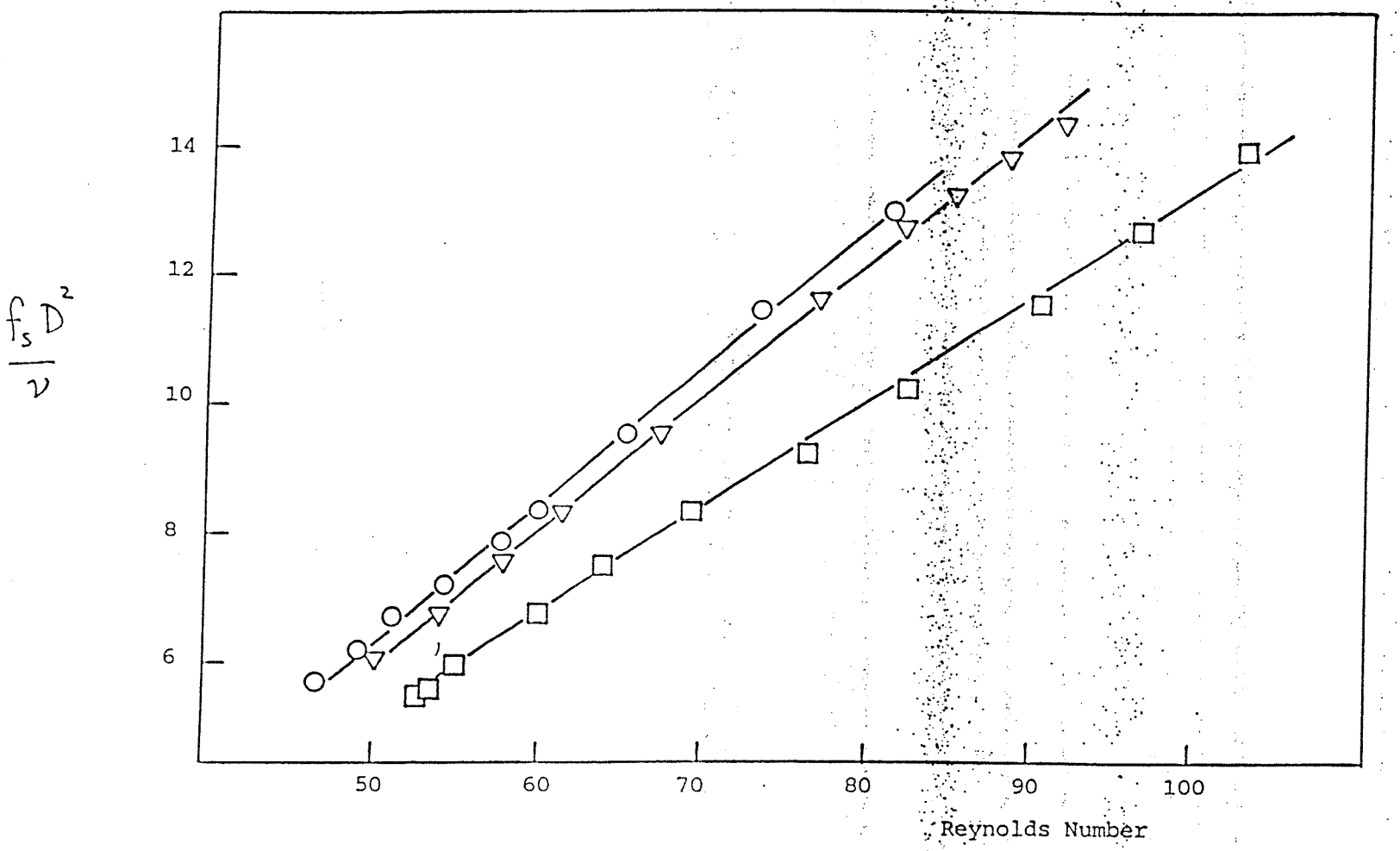

Fig. 11. The variation of the saturation frequency with Reynolds number for three different aspect ratios. ○, aspect ratio 60; ▽, 27; □, 14.

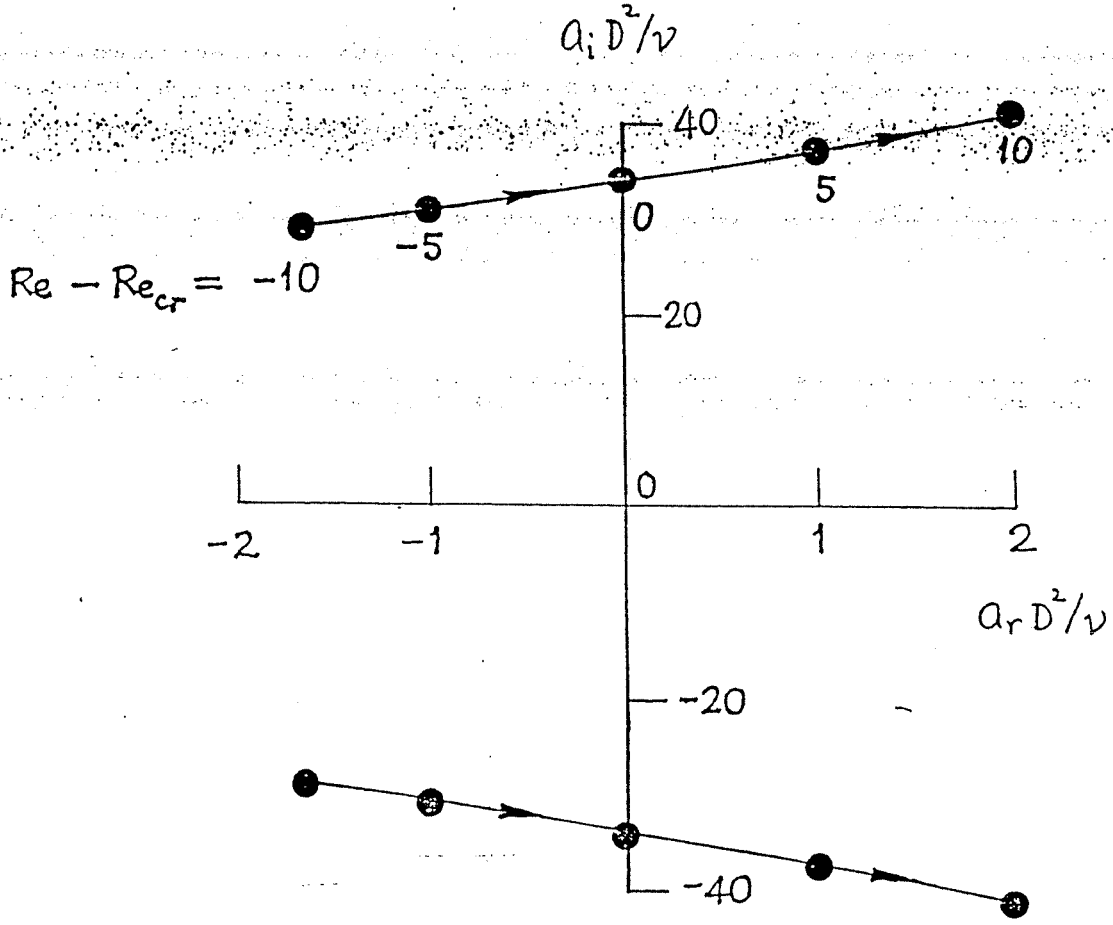

Fig. 12. As the Reynolds number increases from below Re_{cr} to above Re_{cr}, the complex conjugate eigenvalues of the matrix A in (2.1) move from the left half of the plane to the right at a speed given by $d(a_r D^2/\nu)/dRe$.

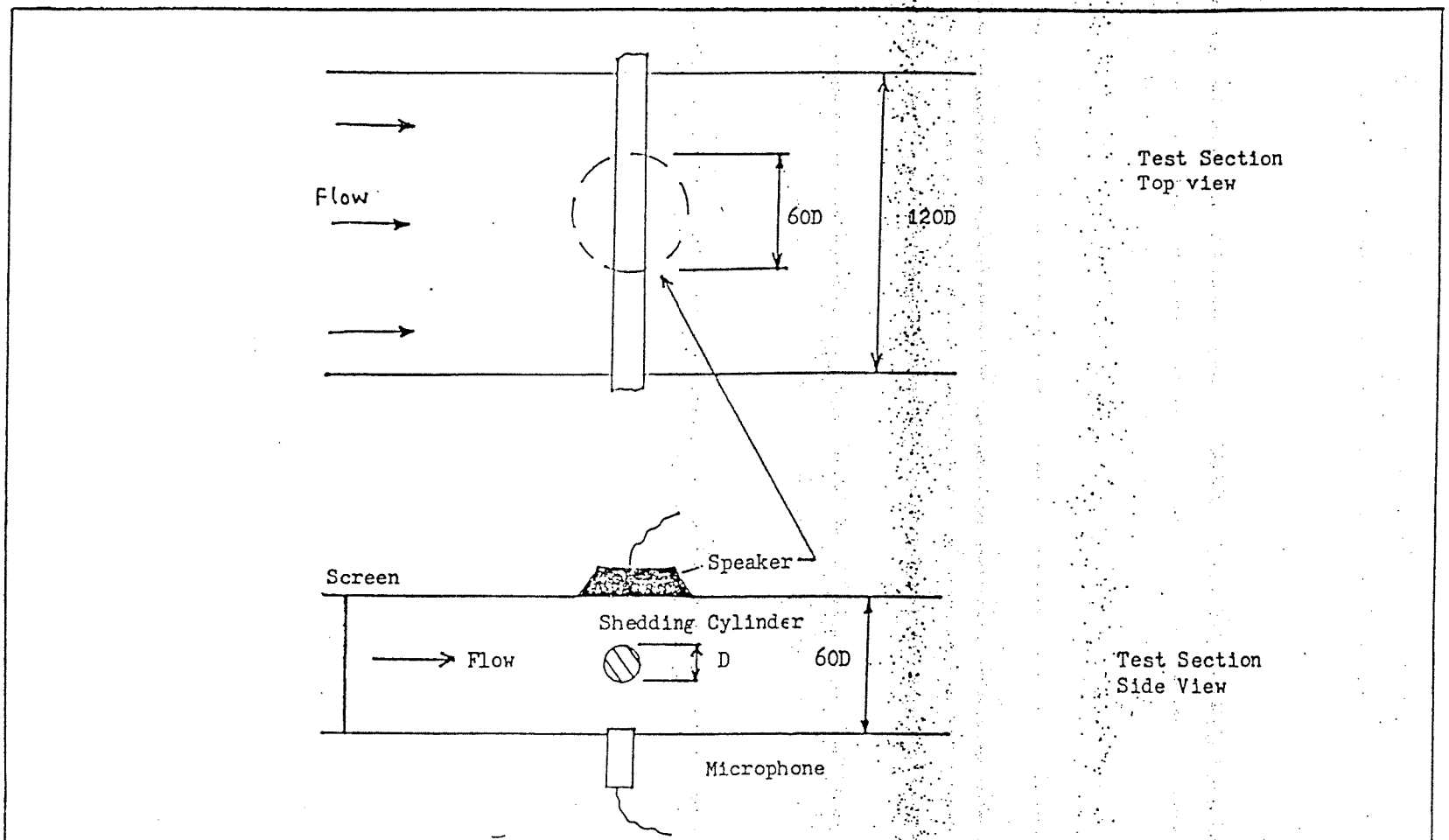

Fig. 13. Schematic of apparatus for the the acoustic excitation work; not to scale.

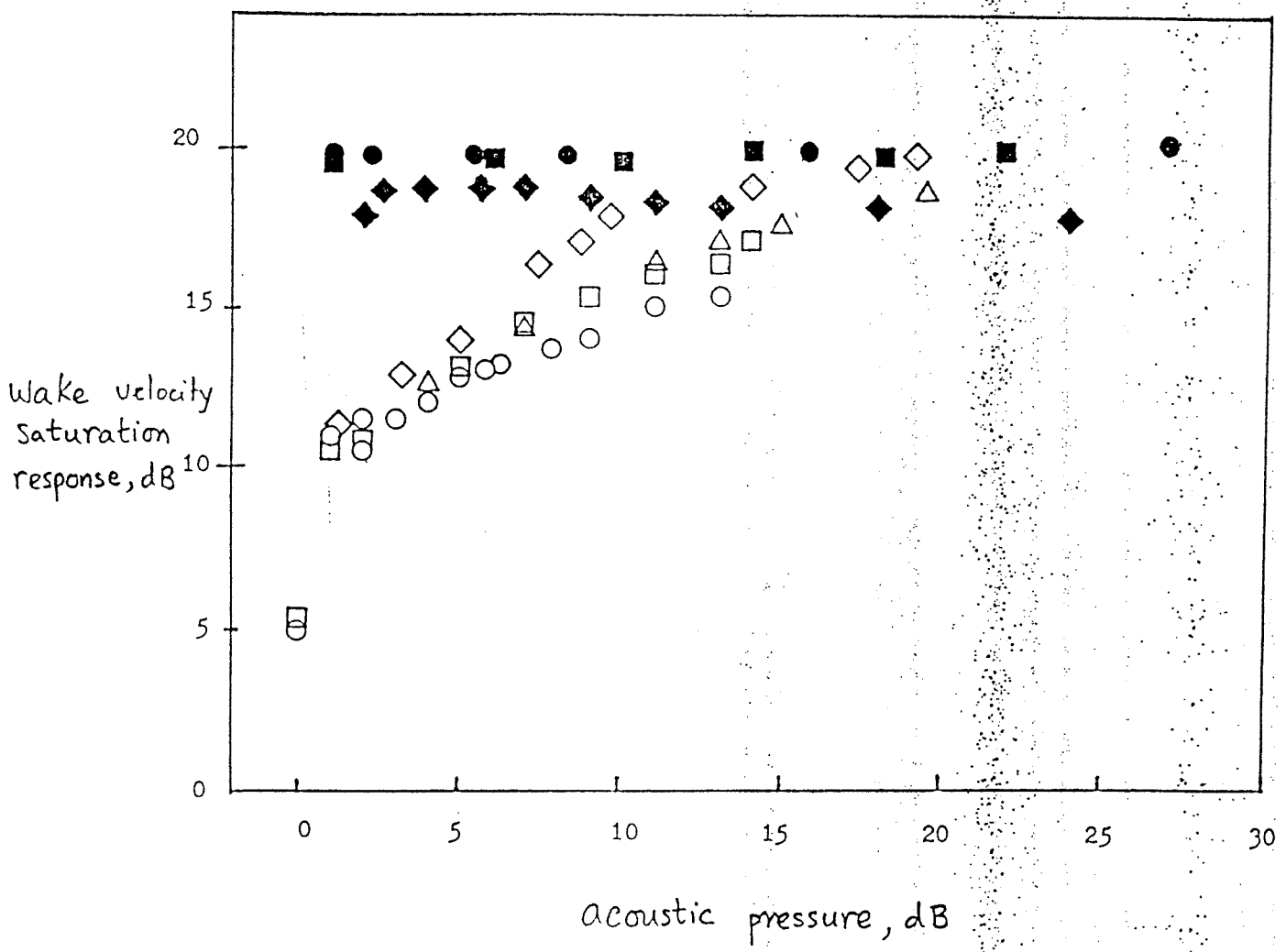

Fig. 14. Wake saturation amplitude *vs* external acoustic excitation. Both axes are in logarithmic scales to base 10. Hot wire position x/D = 10, y/D = 1.0, Re = 27; □ , Re = 30; Δ , Re = 36; ♦ , Re = 46; ■ , Re = 51; ● , Re = 61.

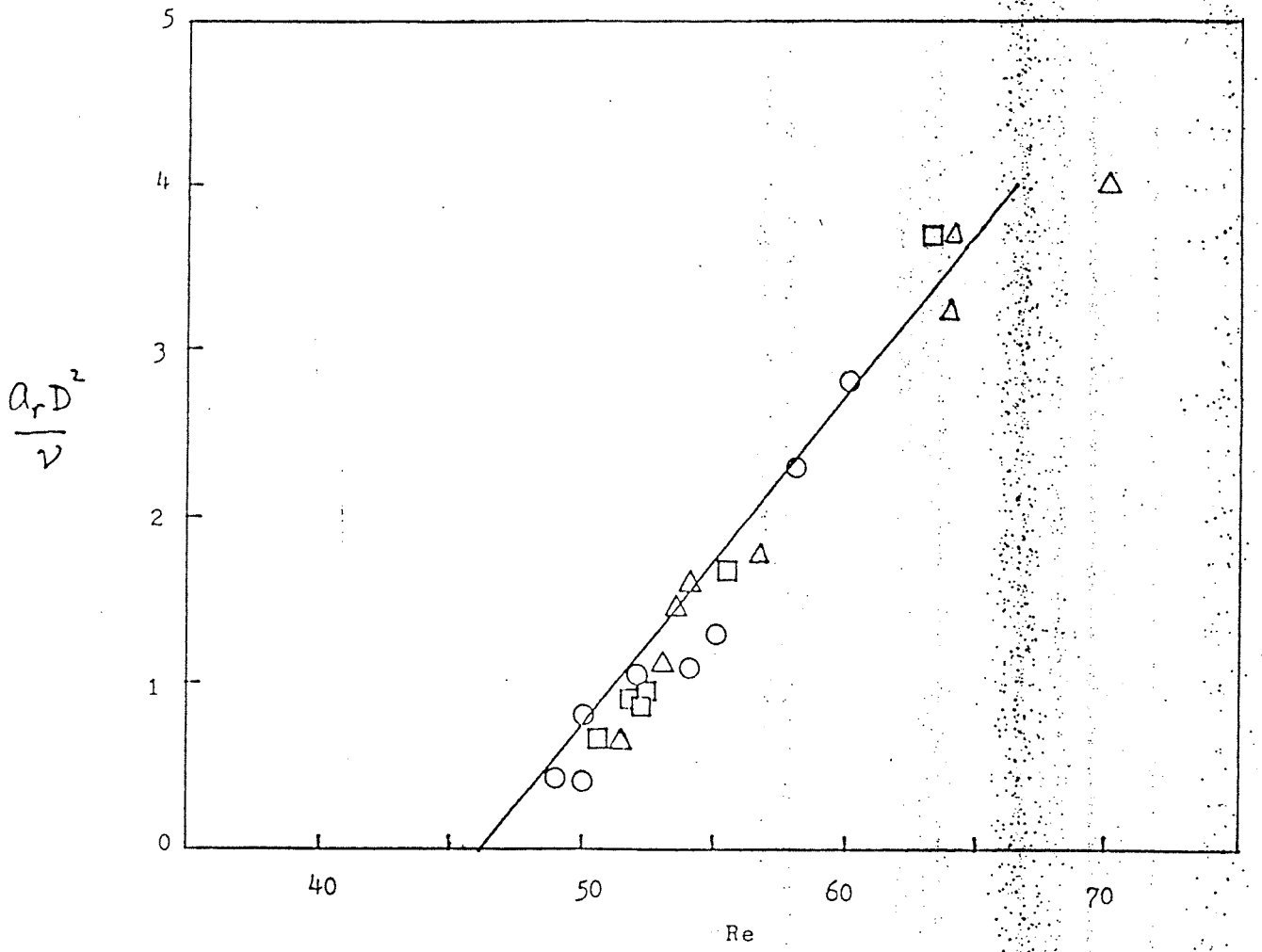

Fig. 15. Growth rates at different freestream turbulence levels. ○, turbulence level of 0.09%; □, 0.16%; △, 0.19%. The continuous line corresponds to equations (4.3), and is a good fit to data obtained at a turbulence level of 0.03%.

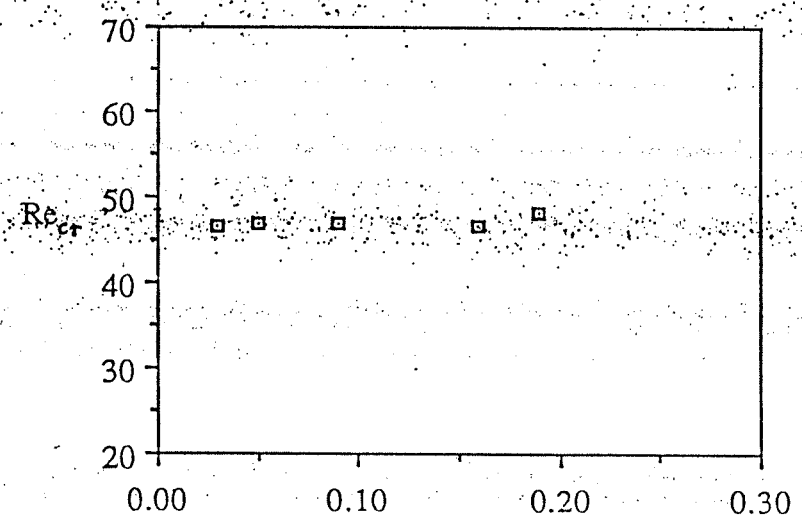

Fig. 16. Critical Reynolds numbers as a function of the freestream turbulence level